CADMIUM PLASMA RECOMBINATION LASER

by

ALIKA KHARE

DEPARTMENT OF PHYSICS

INDIAN INSTITUTE OF TECHNOLOGY KANPUR

AUGUST, 1987

CADMIUM PLASMA RECOMBINATION LASER

A Thesis Submitted
in Partial Fulfilment of the Requirements
for the Degree of

DOCTOR OF PHILOSOPHY

by

ALIKA KHARE

to the

DEPARTMENT OF PHYSICS

INDIAN INSTITUTE OF TECHNOLOGY KANPUR

AUGUST, 1987

CERTIFICATE

Certified that the work contained in this thesis entitled "CADMIUM PLASMA RECOMBINATION LASER" has been carried out by Ms. Alika Khare under my supervision and the same has not been submitted elsewhere for a degree.

R K Thareja

(Dr R K THAREJA)
Thesis Supervisor

Kanpur

August 5, 1987

ACKNOWLEDGEMENT

I am deeply grateful to Dr R K Thareja for introducing me to the subject, his supervision and keen interest during the course of work. Working with him has been a rich experience and shall always be a pleasant memory.

I am thankful to all the members of our laboratory for their cooperation. I wish to thank Anshu, Rama, Rekha and Vinay who made my stay enjoyable at IIT Kanpur.

Technical assistance of the members of CELT workshop, glass blowing workshop and optics shop of IIT Kanpur is highly acknowledged.

Thanks are due to Mr G R Hoshing and Mr S L Yadav for typing the manuscript and Mr R K Bajpai for preparing the tracings.

I wish to express my deep sense of gratitude to my parents for their continuous encouragement.

Alika Khare

List of Publications

1. R K Thareja and Alika Khare, "A Pulsed Metal Vapor Recombination Laser" Opt Lett, **12**, 28 (1987).
2. Alika Khare and R K Thareja, "Performence Characteristics of Pulsed Metal Vapor Recombination Laser" J Appl Phy **XX** XX (1987)
3. Alika Khare, V Kumar and R K Thareja, "On Studies of Spontaneously Emitted Cd I and Cd II Lasing Transitions" J Phys D, At Mol and Clusters **XX** XX (1987).
4. Alika Khare and R K Thareja, "On Gain Scaling of Recombination Lasers" J Appl Phys (submitted).
5. Alika Khare and R K Thareja, "Gain Measurement of Cd Recombination Laser" Appl Opt, (submitted).
6. Alika Khare and R K Thareja, "On Studies of Cadmium Recombination Laser" IEEE J Quant Elect (submitted).

TABLE OF CONTENTS

List of Figures

List of Tables

Page

List of Symbols

α	Three body collisional recombination coefficient.
α_r	Two body radiative recombination coefficient.
τ_+	Characteristic recombination time of an ion.
ϵ_r	Energy evolved as a result of recombination.
η	Reduced population (z scaling).
Θ	Reduced temperature (z scaling).
λ	Wavelength.
σ_{ea}	Elastic scattering cross-section.
τ_d	Delay between peak of appearance of laser pulse and current.
ξ	Angle of rotation.
A(u,l)	Transition probability.
c	Velocity of light.
e	Electronic charge.
E_i	Binding energy of level i.
E_{ul}	Energy difference between level u and l.
E_H	Ionization potential for hydrogen atom.
f(u,l)	Oscillator strength.
g_i	Statistical weight of level i.
g(v)	Line profile.
G_{ul}	Small signal gain.
h	Planck constant.
I	Intensity.

I_p	Ionization potential.
J_i	Net rate of collisional transition for level i.
k	Boltzman constant
K_{ie}	Rate constant for collisional ionization.
K_{ei}	Three body recombination into level i.
L	Variable loss introduced into cavity.
m_e	Electron mass.
M	Atomic mass
M_B	Mass of background gas atom.
M_m	Highest excited level.
n_B	Background gas atom density.
n_e	Electron density.
n_i	Atomic density of level i.
n_i^B	Boltzman population for level i.
n(z+)	Density of ions in charge state z.
n_+	Ion density.
$Q_{\Delta T}$	Loss of energy in elastic collision between electron and buffer gas atom.
Q_{inel}	Loss of energy due to inelastic collision.
R_1, R_2	Mirror reflectivities.
R_i, R_{ij}	Resistances representing collisional transitions.
R_l	Decay rate of lower laser level.
R_u	Decay rate of upper laser level.
S_i	Source term representing processes other than collisional and radiative processes.

T_B	Transmission through each window.
T_e	Electron temperature.
ν	Frequency of transition.
ν_e	Reduced population density of electron.
ν_i	Reduced population density of level i.
W_{ij}	Normalized rate constant.
$X(T_e,u,l)$	Collisional de-excitation coefficient from level u to level l at temperature T_e.
z	Charge on ion.

SYNOPSIS

CADMIUM PLASMA RECOMBINATION LASER

Submitted in partial fulfilment of the requirment
for the degree of

DOCTOR OF PHILOSOPHY

by

Alika Khare

to the
DEPARTMENT OF PHYSICS
INDIAN INSTITUTE OF TECHNOLOGY
KANPUR 208 016 INDIA

In this thesis we report the development of and studies on performance characteristics of Cadmium Plasma Recombination Laser.

The electrode arrangement of the system developed consists of a large number of cadmium strips positioned end to end on a glass substrate so as to leave a spacing of 1 mm between adjacent strips. This electrode arrangement was sealed in a glass tube having Brewster windows. Two extreme end strips were used for connection to high voltage power supply. Two types of excitation circuits were used. i RC circuit and ii LC circuit. Helium was used as buffer gas for most of the investigations. However, to see the effect of other background gases we tried neon, argon and mixtures of helium and neon gases also. Laser

resonator was formed by using two two meter radius of curvature mirrors of high reflectivity. The laser output was detected using Ge detector and photomultiplier tube for IR and visible radiation respectively. The output signal was fed onto the oscilloscope/boxcar averager and recorded on chart recorder.

Laser action was observed on 6p $^3P_2$ - 6s $^3S_1$ at 1.40 μm, on 6p $^3P_1$ - 6s $^3S_1$ at 1.43 μm and on 4f $^3F_4$ - 5d $^3D_3$ at 1.65 μm transitions of Cd I and on 4f $^2F_{5/2}$ - 5d $^2D_{3/2}$ at 533.7 nm and on 4f $^2F_{7/2}$ - 5d $^2D_{3/2}$ at 537.8 nm transitions of Cd II based on recombination pumping in a sealed discharge tube. We report for the first time , the performance characteristics of the observed transitions over a range of discharge parameters in the presence of low pressure background gas, resonator axis and the length of the gain medium. The optimum value of resonator axis is found to be 8 mm away and parallel to the row of metal strips. To see the effect of the length of the active medium on laser output power, experiment was performed with 10, 40 and 70 plasma segments. Peak laser output power is observed to increase with the number of plasma segments. Laser action is observed in the afterglow. Delay between the peak of laser pulse and the current pulse is observed to be as much as 170 μs for Cd I transitions and 30 μs for Cd II transitions. Peak laser output power P_o is found to be dependent on current. Initially P_o increases with current, attains a maximum value and then decreases with further increase in current. Optimum value of current required for

observing visible laser is higher than that for IR laser. LC circuit is found to be more efficient than RC circuit for observing laser action in our configuration. Helium being lightest of all the gases and of high ionization potential is found to be the best candidate as background gas in our configuration. The optimum value of helium pressure is found to be dependent on lasing transitions under consideration, number of plasma segments and the energy dumped into the system. With increase of number of plasma segments, the optimum value of helium pressure decreases for the same input energy. It is observed that the optimum value of helium pressure required for Cd II transitions is lower than that for Cd I transitions. An attempt is also made to scan the radial profile and is compared with a theoretical fit for IR laser.

Small signal gain of the laser was estimated by introducing variable losses into the cavity. Our experimental values of small signal gain are 8.7 (-3) cm^{-1}, 7.1 (-3) cm^{-1} for 1.65 μm and 1.43 μm transitions respectively and 6.0 (-3) cm^{-1} for visible transition at 537.8 nm. Plasma temperature is estimated by comparing the intensities of emitted visible cadmium lines. The temperature is estimated to be in the range of $0.5 \text{ ev} \leq T \leq 1.0$ ev for Cd I and $1.0 \text{ ev} \leq T \leq 2.0$ ev for Cd II transitions. The results are in agreement with the computed values based on proposed electric network model under collisional recombination conditions.

Chapter 1

INTRODUCTION

The possibility of obtaining the laser action in a recombining plasma was first suggested by Gudzenko and Shelepin [1] in 1964. They considered a supercooled hydrogen plasma as active medium. Recombination laser was first observed experimentally by Latush et al [2] in 1973 in Ca and Sr in an afterglow discharge. Since then there have been many reports [3-20] on the calculation and observation of the population inversion in a recombining plasma from IR through X-ray region in neutral, singly and multiply ionized species. In recombination lasers, the population of the levels are determined by the collisional radiative processes [21], involving recombination of free electrons with ions followed by collisional and radiative de-excitation of the captured electrons. Detailed calculations for recombining hydrogen [3,4], hydrogenic ions [5], helium [6-8], lithium [9], carbon [10-14],aluminium [16], potassium [17], and xenon [18] plasmas confirmed that significant population inversion can be established whenever the free electrons cool in a time short compared to the relaxation time of the ground state of atoms or ions involved. However, there are only a few reports [2, 22-28] on the observation and studies of recombination laser.

Plasma recombination laser has following potential advantages:

(i) The mechanism is applicable to transitions involving atomic as well as ionic species. It offers a possibility of

having devices with operating wavelengths from infrared, through X-ray region.

(ii) Capability of either pulsed or CW operation.

(iii) The physical state of plasma does not change at high densities of pump energy, therefore, there is a possibility of developing more powerful and efficient lasers.

Excitation Mechanism

The excitation mechanism of a plasma recombination laser can be explained with the help of Fig 1. First, the ions of an active element are created in some charge state z by feeding some energy into the medium. Input energy may be from an eletrical discharge an arc or a laser beam or an electron beam. Large amount of energy required to disturb the thermal equilibrium of level populations results in highly ionized plasma. Electrons are cooled by allowing it to expand or by collisions with atoms of some background gas and recombine with ions to go to some highly excited levels of the next lower charge state z-1. These bound electrons move downward via collisions with the background gas atoms until a significant gap in the energy level is reached where the collisional decay rate is significantly reduced. Due to the reduced collisional decay rate across the gap, the population will start building up just above this gap. An inversion would occur with respect to one or more lower levels resulting in laser action across the gap provided the decay rate of the lower level is fast. The lower laser level may decay by either of the two

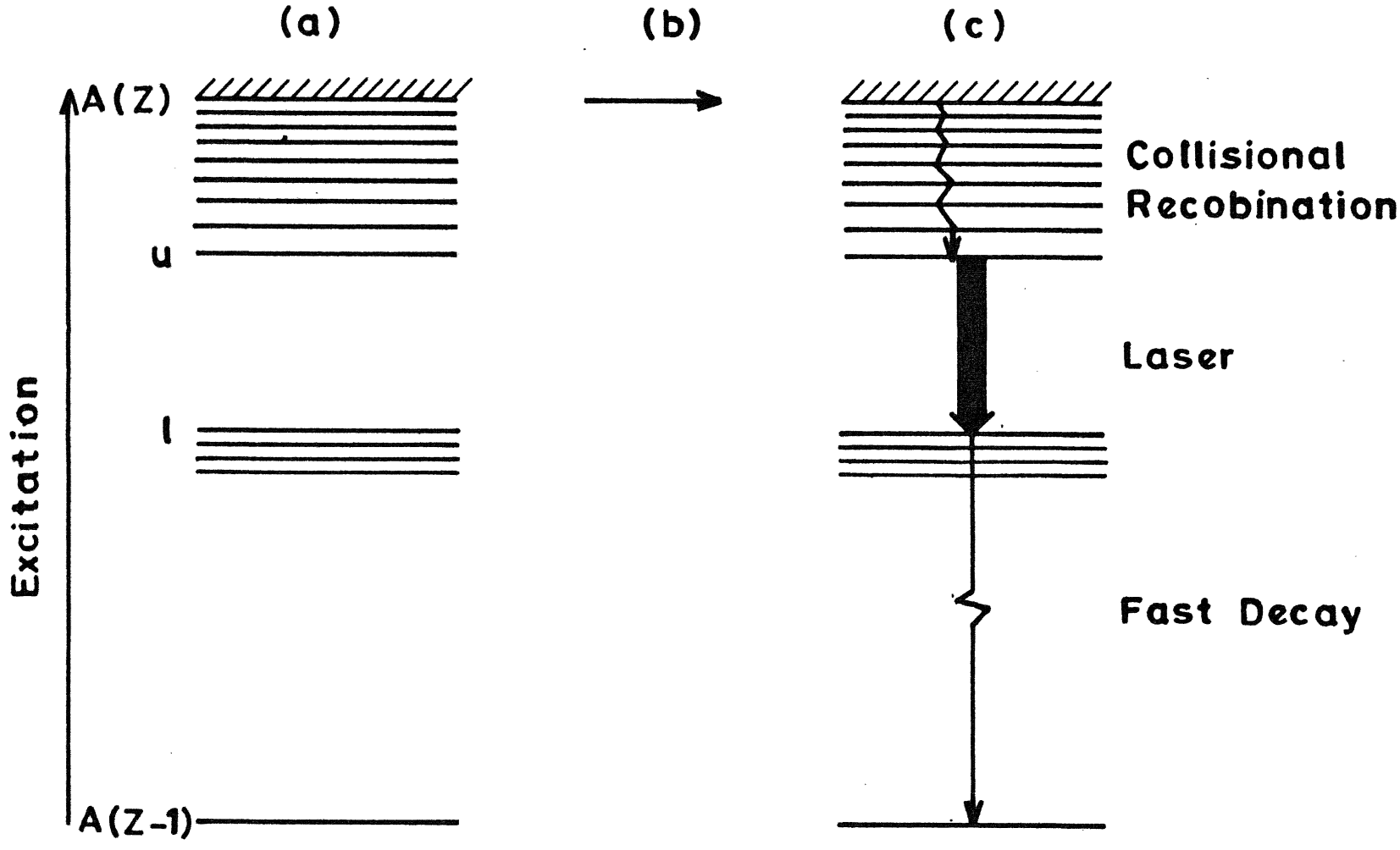

(a) Creation of Plasma (b) Cooling (c) Decay

Fig. 1 Schematic energy level diagram for a plasma recombination laser

processes (i) radiative decay or (ii) collisional decay, depending on particular choice of the atomic species and plasma conditions.

Under recombination conditions, the laser action takes place between two groups of closely spaced levels, the gaps between such groups are considerably greater than the seperations between the levels with in a group as shown in Fig 1. The upper level is the lowest level of the upper group and the lower level is the upper most level of the lower group. If the electron temperature (kT_e) is less than the spacing ΔE between closely spaced levels ($kT_e \leq \Delta E$), the population densities of these closely spaced levels can be assumed in thermal equilibrium with an electron temperature T_e among themselves. Therefore, one can assume a recombination laser to be a two level system with upper level u and lower level 1. The rate of change of population density of these two levels is

$$\frac{dn_u}{dt} = \frac{n_+}{\tau_+} - R_u n_u \qquad 1$$

$$\frac{dn_1}{dt} = R_u n_u - R_1 n_1 \qquad 2$$

where n_u, n_1, n_e and n_+ are the population densities of upper level, lower level, electron and the ion respectively, τ_+ is the characteristic recombination time of an ion, R_u and R_1 are the decay rates of upper and lower laser level respectively. Recombination process is described by equation

$$A(z) + e + e \longrightarrow A(z-1) + e$$

Rate of change of electron and ion density is

$$\frac{dn_+}{dt} = -\alpha n_+ n_e^2 = \frac{dn_e}{dt} \qquad 3$$

It follows from eq 3 that characteristic recombination time of an ion is

$$\tau_+ = (\alpha n_e^2)^{-1} \qquad 4$$

where α is the collisional recombination coefficient given by [29]

$$\alpha = 9.2 \times 10^{-39} z^3 T_e^{-9/2} \ln \sqrt{(z^2+1)} \qquad 5$$

$$= C(z) T_e^{-9/2}$$

where $C(z) = 9.2 \times 10^{-39} z^3 \ln \sqrt{(z^2+1)}$

Under steady state condition, from eqs 1,2,4 and 5, it follows

$$\Delta n_{u1} = n_u - n_1$$

$$= \frac{n_+ n_e^2 C(z) T_e^{-9/2}}{R_u} \left(1 - \frac{R_u}{R_1}\right) \qquad 6$$

The expression for small signal gain [30] is

$$G_{u1} = \frac{c^2}{8\pi\nu^2} A(u,1)\, g(\nu)\, \Delta n_{u1}$$

using eq 6

$$G_{u1} = \frac{c^2}{8\pi\nu^2} A(u,1)\, g(\nu) \frac{1}{R_u} n_+ n_e^2\, C(z)\, T_e^{-9/2} \left(1 - \frac{R_u}{R_1}\right) \qquad 7$$

Where c is the velocity of light, ν is the frequency corresponding to the transition under consideration, A(u,1) is the transition probability and g(ν) is the line profile factor.

Thus to achieve large population inversion and hence gain, it follows from eq 6,

1. $R_1 > R_u$, fast decay of the lower laser level.

2. $T_e^{-9/2}$ dependence implies low electron temperature, hence fast cooling of plasma.

3. Large plasma density (n_e, n_+).

The first factor is dependent on the energy level scheme under consideration as well as on the plasma conditions.

The second factor on which population inversion depends is the electron temperature, the rate of change of electron temperature in the afterglow is given by [31]

$$\frac{d\ (3/2\ kT_e n_e)}{dt} = -Q_{\Delta T} + \epsilon_r\ \alpha n_e^3 + Q_{inel} \qquad 8$$

where $Q_{\Delta T}$ is the loss of electron energy in elastic collision between electrons and buffer gas atoms, ϵ_r is the energy evolved as a result of recombination and Q_{inel} is the transfer of energy to the electrons due to inelastic collisions [31]. In the afterglow, the electron density changes much more slowly than the electron temperature. Therefore, eq 8 can be considered as the equation for the temporal variation of T_e. The last two terms in eq 8 show the rate of decrease of T_e. They have little effect on electron temperature. Therefore, electron temperature is dominated by the first term. The elastic collision with the buffer gas atom is given by [32]

$$Q_{\Delta T} = \frac{2m_e}{M_B} \sigma_{ea} n_B \left(\frac{8kTe}{\pi m_e}\right)^{1/2} \qquad 9$$

where σ_{ea} is the elastic scattering cross-section between electrons and atoms [33], M_B is the mass of the buffer gas atom and n_B is the density of buffer gas atoms. It follows from eqs 8 and 9 that rate of cooling is inversely proportional to M_B, it implies that the cooling process will be efficient for lighter buffer gas. Helium is the lightest inert gas and, therefore, in the case of elastic collisions with helium atoms or ions the electrons give up relatively a large part of their energy resulting in strong recombination into the excited levels. Hydrogen being lightest gas, one would expect it to be more efficient. Since its ionization potential is low, part of the exciting energy is used up to ionize the hydrogen gas also. We tried He, Ne, Ar and mixture of He and Ne as the background gas. Helium was found to be the best background gas for observing cadmium plasma recombination laser in our configuration.

The third factor in eq 6 determining the population inversion is the plasma density. A high initial plasma density will be required for large population inversion. However, an optimum value of plasma density [22, 34] is somewhat lower. The lower density is needed to minimize the unwanted collisional depopulation of the upper laser level. An upper limit on the electron density can be obtained by equating the collisional de-

excitation rate to the radiative decay rate [21, 35],

$$n_e\, n_u\, X(T_e,u,l) = n_u\, A(u,l)$$

$$n_e = \frac{A(u,l)}{X(T_e,u,l)} \qquad 10$$

where $A(u,l)$ is the radiative transition probability from level u to level l and $X(T_e,u,l)$ is the collisional de-excitation coefficient from level u to level l at electron termperature T_e and is given by [35]

$$X(T_e,u,l) = \frac{g_l}{g_u}\,\frac{6.5\times10^{-4}}{E_{ul}\,T_e^{1/2}}\,f(u,l) \qquad 11$$

where $f(u,l)$ is the oscillator strength and E_{ul} is the energy difference between the levels involved, g's are the statistical weight of the levels. From eqs 10 and 11

$$n_e = \frac{8\pi^2\, e^2}{m_e c^3\, 6.5\times10^{-4}}\,E_{ul}\,T_e^{1/2}\,\nu^2$$

$$= \frac{0.123\,T_e^{1/2}}{\lambda^3_{ul}} \qquad 12$$

where λ_{ul} (cm) is the wavelength corresponding to the transition under consideration.

Equation 12 gives an upper limit to the electron density for a recombination laser.

Difference between Plasma Recombination Lasers, Gas Lasers and Metal Vapor Lasers

The conventional gas lasers e.g. Ar ion, Xe ion etc also utilize ionized gas. In gas lasers, the active medium is ionizing plasma whereas in plasma recombination lasers,the active medium is recombining plasma. The deviation of the active medium from thermodynamic equilibrium [36] is different in two cases. In a gas laser, the electrons are overheated. The free electron number density is less than Saha value for the local electron temperature. In the case of plasma recombination laser, the electrons are super cooled, the free electron density is appreciably greater than the Saha value for the local electron temperature [31]. Because of this difference, the gas lasers use leading edge of the excitation pulse, whereas plasma recombination lasers utilize the afterglow region. Active medium for a recombination laser can be metal vapors. The metal vapor recombination lasers differ from the conventional metal vapor lasers, e.g. He-Cd laser. In metal vapor lasers, a buffer gas, usually helium, is used which takes part in pumping process through collisions, penning ionization [37-41]. In recombination lasers the cooling of the free electrons in the afterglow is usually achieved by using inert gas e.g. helium; which takes away the excess energy of electrons via collisions and brings them downwards to populate the upper laser level.

Efficiency of a Recombination Laser

It follows from eq 6 that a recombination laser requires the production of high density plasma, followed by rapid cooling and recombination of electrons and ions to next lower charge state to give population inversion. Therefore, the efficiency of a recombination laser is dependent on the efficiency with which the required upper laser level is populated in given plasma conditions (electron density, temperature etc.). Define a parameter r as the ratio of the upper laser level population n_u to the electron density n_e

$$r = \frac{n_u}{n_e} \qquad 13$$

Since the pumping source for a plasma recombination laser involving the (z-1) charge state being the density of ions in the next higher charge state z, one can split r into two parts,

$$r = \frac{n(z+)}{n_e} \; \frac{n_u}{n(z+)} \qquad 14$$

The first factor on the right hand side of eq 14 defines the efficiency with which ions in the proper charge state are produced. The production of ions is an unknown factor experimentally as well as theoretically [42]. There are two factors which effect the production of ions in the proper charge state. These are distribution of ions in the lower charge states and an early recombination. The first factor can be overcome by keeping the rate of increase of electron density high. The second factor

can be overcome by keeping an upper limit on electron density given by eq 12.

The second factor $n_u/n(z+)$ in eq 14 defines the efficiency with which the ions in the higher charge state recombine to the next lower charge state to populate the required upper laser level. It is dependent on the decay of the ions during recombination phase of plasma. There will be some loss of ions because of diffusion to the walls. This loss can be minimized by keeping the background gas pressure and tube diameter large [43]. Higher buffer gas pressure lowers the electron temperature more rapidly in the discharge afterglow and thus increases the rate of recombination of ions which leads to higher laser peak powers. Secondly an increase of gas pressure increases the discharge impedence and thus enables input energy to be deposited in the active medium from a driving source of fixed impedence which is generally somewhat larger than that of discharge. However, background gas pressure cannot be increased beyond a certain limit, if the pressure is very high, the electrons will loose more energy via collisions resulting in decrease in inversion density.

Another process which effects the efficiency of recombination to the required level is the radiative recombination which may lead to the excitation of levels below the upper laser level. The process is described by

$$A(z+) + e \longrightarrow A(z-1,l) + h\nu$$

where hv is the energy of emitted photon. The radiative

recombination coefficient is given by [44]

$$\alpha_r = (2.7\times10^{-19})\ z^2\ T_e^{-3/4} \qquad 15$$

The most effective process for a recombination laser is the collisional recombination process. The three body colisional recombination coefficient [29,44,45] is given by eq 5. Thus to minimize the radiative recombination process, electron temperature should be kept low and the electron density should be high. But according to eq 12, there is a limit on electron density, beyond which the efficiency of the system will go down. Therefore, electron density should be kept high enough to dominate over the radiative recombination, but simultaneously it should be low enough to avoid the collisional de-excitation from the upper laser level.

The efficiency of a recombination laser, like any other laser is dependent on decay scheme of lower laser level also (eq 6). The main mechanism of depopulation of the lower laser level in a plasma recombination laser are radiative de-excitation and collisional de-excitation. The radiative depopulation is effective when the lower laser level is quite high, the plasma is not too dense and the lasing volume is not very large. In case of atoms, the radiative clearing of the lower laser level is not efficient at high electron density and electron temperature. However, in case of multiply charged ions, it may be an efficient mechanism for clearing of the lower laser level even at high plasma density and electron temperature.

Various Experimental Techniques for Recombination Lasers

Conditions required for a recombination laser can be achieved either cooling the plasma rapidly via collisions with walls [2,46,47] or by producing the plasma in a relatively smaller volume and then letting it to expand adiabatically followed by reduction in density and temperature. Based on the method of initial excitation/ionization or on method used to cool down the plasma to achieve the proper conditions for recombination, one can categories the plasma recombination lasers into following categories.

(i) Afterglow Recombination Laser

This involves the non-equilibrium decay of electric discharge afterglow [2,47-51]. The electrons are cooled by either collisions with walls or by heavy particle collisions or both. Studies of afterglow recombination laser have been done [2,22,46-51] in Mg II, Ca II, Sr II and Ba II in the infrared, visible and UV region of the spectrum. Pulsed high voltage longitudinal discharge was used to create plasma. Maximum power of 400 W at a wavelength of 430.5 nm corresponding to Sr II transition was reported [22,46]. Butler and Piper [47-49] reported the laser action in transversely excited electric discharge in Sr II and Ca II. Recently McLucas and McIntosh [50,51] have reported on a longitudinal discharge heated Sr II laser.

(ii) Direct Nuclear or e-beam Pumping

The plasma can be created by means of some external ionizing source such as electron beam [28] or fission fragments [52]. In nuclear pumping, the medium is ionized by means of MeV heavy charged particles which slow down in and loose energy to the lasing species. Each charged particle creates numerous secondary electrons which ionize the rare gas atoms. These ions collide with atoms of the lasing species, a charge exchange process takes place and the medium is left with highly ionized ions, rare gas atoms and electrons. The recombination relaxation through the excited levels leads to inversion. DeYoung et al [52] have observed laser action in nitrogen at 862.9 nm and 939.3 nm in a mixture of Ne-N_2 using nuclear pumping. Rocca et al [28] have used e-beam pulses of energy 1 to 5 KeV to observe laser action at 1.65 μm and 1.43 μm of Cd I transitions.

(iii) Plasma Dynamic Laser

Another method of cooling the electrons is to make use of an adiabatically expanding plasma to establish the recombination conditions. In a free expansion, fast electron cooling is achieved, it is accompanied by an even faster decay in electron density. Hence a very high initial plasma density is required to achieve proper conditions of population inversion. Gudezenko et al [53] have suggested a plasma jet arrangement to provide steady or quasi steady expanding plasma flow of the proper species to achieve the recombination conditions. Campbell et al

[26,54] were the first to observe such quasi-steady plasma dynamic laser in argon. A highly ionized argon plasma was formed by injecting argon gas via a high speed solenoid valve into an arc chamber and then cooled down by expanding the flow into a suitable vacuum chamber. Laser was observed in hydrogen [55] and in cadmium [56]. Population inversion has also been observed in recombining hydrogen [57] and helium [8,58] plasma jets.

(iv) Laser Produced Plasma Recombination Laser

This method employs both cooling processes, due to adiabatic expansion as well as due to the collision with buffer gas atoms. This method overcomes the problem of reduction in plasma density as a result of free expansion by confining the plasma expansion in presence of buffer gas. In this scheme, high density plasma is created within a small volume by focussing a high power laser radiation on to the target material. High density plasma expands, cools and recombines to give laser action. Silfvast et al [24,25] were first to demonstrate this scheme to obtain laser oscillations. Laser oscillations in Ar, Kr, Xe gases and their mixtures [59] and in Cd [24] in presence of low pressure helium gas have been observed in the expanding phase of transversely created laser produced plasma using CO_2 and Nd-YAG lasers. Small signal gain has been observed at XUV wavelength in C VI [11-13] at 18 nm and in Al XII at 13 nm [16] in Nd laser produced plasma expanding in vacuum.

(v) Segmented Plasma Excitation and Recombination Laser

This scheme utilizes both the cooling mechanisms, expansion as well as collision processes. Plasma is created by feeding electrical energy into the system. Segmented plasma excitation and recombination (SPER) laser was first suggested [61] in 1980 . Laser oscillations have also been reported in cw mode [62] in similar configuration. Helium was used as a background gas in continuously flowing mode. We have employed the similar technique to observe laser action for present work [63,64]. Helium, neon, argon and mixture of helium and neon gases were used as background gas in a sealed discharge system.

The electrode arrangement in our system consists of a large number of thin metal strips placed end to end on an insulated substrate so as to leave spacing (~ 1mm in our case) between adjacent strips. A high voltage high current pulse is applied across the end strips to create the metal vapor plasma in each gap. A low pressure of background gas, usually helium, is used. It helps in producing metal vapor in the gap region, controls the subsequent expansion of the vapors, and cools the recombining electrons, causing electron ion recombination to occur in the plasma as they expand away from the gaps. Laser resonator with axis parallel to row of gaps is formed with two dielectric coated mirrors of high reflectivity. There is a restriction on gap spacing also. As the gap spacing increases, more helium is excited in the gap resulting in decrease in laser output. It

has been found that gap spacing should be somewhere near the thickness of the metal strips [61,63]. Thin strip of metal is preferred because it has advantage over the bulk electrodes. Thin electrodes provide an increased ionization growth rate and larger metal vapor density in the gap region than the bulk electrodes because of the enhanced thermal processes that act at the surface of thin electrodes during the early stages of the breakdown. With the bulk electrodes, the heat flow from electrode surface into the metal is three dimensional, but in thin geometry, the heat flow is nearly two dimensional. Hence heat loss due to conduction is less for thin electrodes and therefore, surface temperature of thin electrode increeases more rapidly than the surface temperature of a bulk electrode, resulting in greater metal vapor production [65].

Since vapors are used to provide the atomic species, therefore high vapor pressure materials would be most desirable. It follows from eq 6 that to achieve population inversion, the concentration of recombining ions should be as high as possible. Therefore, active atoms should be of low single and double ionization potential. The best candidates for laser being alkaline earth metals.

Present Work

In the present work, we have used segmented plasma excitation and recombination scheme in a sealed system to observe the laser action in Cd I and Cd II transitions with He, Ne, Ar

and mixture of He and Ne as background gas.

The details of the experimental techniques used in the present work are described in Chapter 2.

Chapter 3 describes the results of present work on IR laser. The characteristics of laser corresponding to 1.65 μm and 1.43 μm transitions of Cd I are studied. Behaviour of laser as a function of resonator axis (the distance from metal surface) pressure of He, Ne, Ar gas, plasma current, shape of the current pulse, voltage and the total energy dumped into the system is reported. An attempt is made to scan the radial profile of the laser. Gain is estimated experimentally and studied as a function of plasma current and background gas pressure.

Chapter 4 describes the results of visible laser transitions corresponding to 533.7 nm and 537.8 nm transitions of Cd II. The effect of length of the active medium is investigated. Behaviour of laser output as a function of plasma current and background gas pressure is presented. Results are compared for Cd I and Cd II transitions.

The calculations for small signal gain are given in Chapter 5. Gain is calculated under recombination conditions using electric network model originally proposed by Bates [66] and later extended by Lawless [67]. In this model, the collisional processes are considered in terms of passage of steady current through a network of linear conductors and resistors, the processes other than collisional processes are represented by a

source term which represents the current introduced into the system. Based on our model we have evaluated the gain for C VI and hydrogen and compared with earlier reports [10,13]. Experimentally observed small signal gain for Cd I and Cd II transitions and electron temperature are compared with the theoretical values estimated using the proposed model.

Chapter 6 summarises the results of present work.

Chapter 2

EXPERIMENTAL TECHNIQUE

Various experimental schemes for a plasma recombination laser have been described in Chapter 1. We have developed a pulsed cadmium plasma recombination laser based on Segmented Plasma Excitation and Recombination pumping scheme. This is the simplest configuration among all the existing configurations. Unlike other metal vapaor lasers e.g. He-Cd laser, it doesn't require any additional heating arrangement to create the metal vapors. In this configuration, a large number of plasma segments were created by applying a high voltage, high current pulse across the ends of a row of metal strips as shown in fig 2. Cadmium used in our system was 99.999% pure (Nuclear Fuel Complex, Hyderabad). Cadmium metal was rolled down to a thickness of nearly 1 mm. Strips of length 10 mm and 2 mm wide were cut of the rolled material. These strips were cleaned properly and pasted on glass substrate end to end so as to leave a spacing of 1 mm between adjacent strips. We have used 10, 40 and 70 gaps for investigations. The length of the end strips were kept around 5 cm, so that free ends could be used for connecting to high voltage. This electrode arrangement was inserted in a pyrex glass tube of outer diameter 45 mm and thickness 2 mm. Tube was terminated at Brewster angle. Before inserting the electrode arrangement, the discharge tube was cleaned thoroughly. Free ends

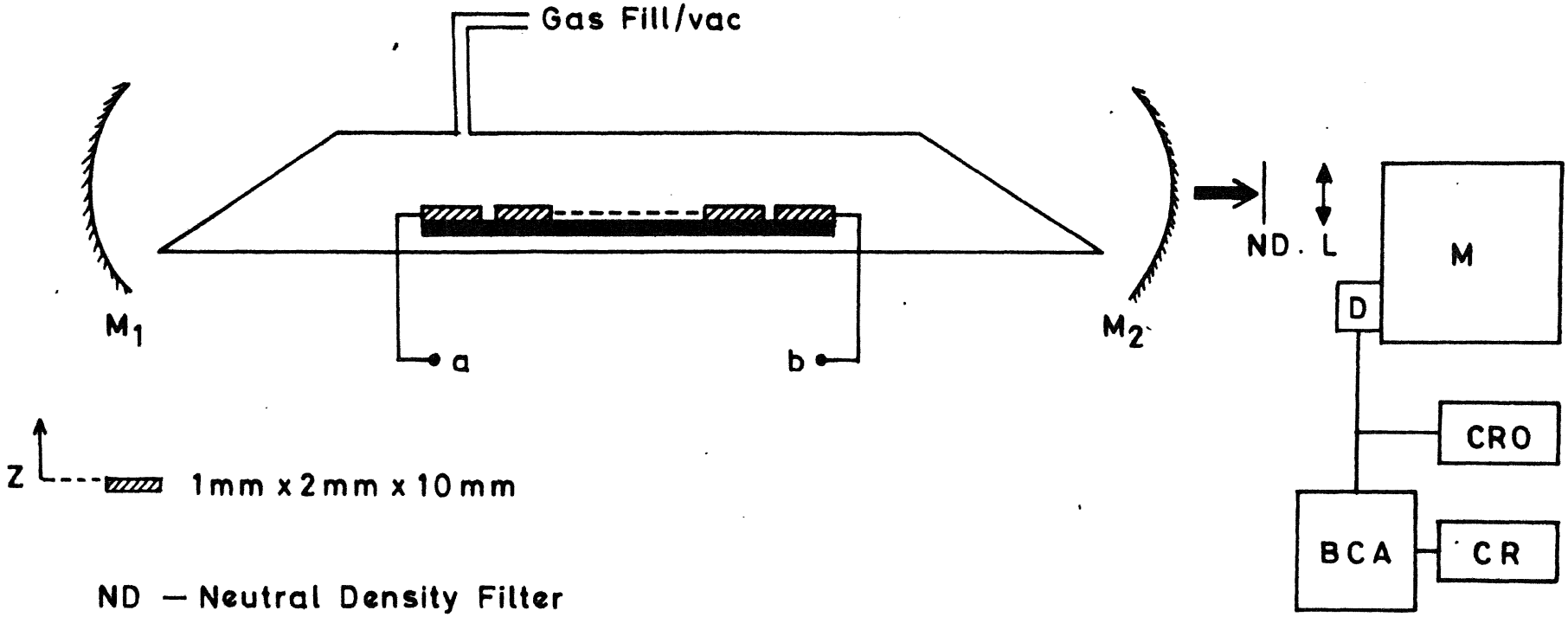

ND — Neutral Density Filter
L — Lens
M — Monochromator
D — Detector
CRO — Cathode Ray Oscilloscope
BCA — Box Car Averager
CR — Chart Recorder

Fig. 2 Experimental arrangement

of the end strips were taken out from two holes drilled in the glass tube. The position of holes, length of the tube, depended on the number of plasma segments used. Free ends of the end strips were connected with the crocodile clips to the discharge circuit. Windows were attached to the ends of the discharge tube by epoxy. Discharge tube was connected to the vacuum system and gas filling arrangement through stopcocks. The vacuum system consisted of an oil diffusion pump and rotary pump. Gas filling arrangement consisted of bulbs of argon and neon gas. An empty glass bulb was used as a reservoir for helium gas. Glass bulb was evacuated to a pressure of 10^{-5} Torr and then filled in at 10 Psi of helium gas from helium cylinder connected to the system. Pressure of the background gas in the discharge tube was monitored with an oil manometer. When the electrode arrangement was new, it was difficult to get cadmium plasma at few torr of helium gas. To get plasma we had to fill in helium at a pressure of around 5 Psi from the helium cylinder. After running the discharge for some time under above conditions, discharge tube was evacuated to a pressure of $\leq 10^{-4}$ Torr and filled in with the required gas at required pressure.

We have used two types of exciting circuits :

i. RC Circuit . It is a simple capacitor discharge circuit as shown in Fig 3. A capacitor was charged through a resistance (24 MΩ) from the high voltage power supply and discharged through the discharge tube with a spark gap as switch. Two values of

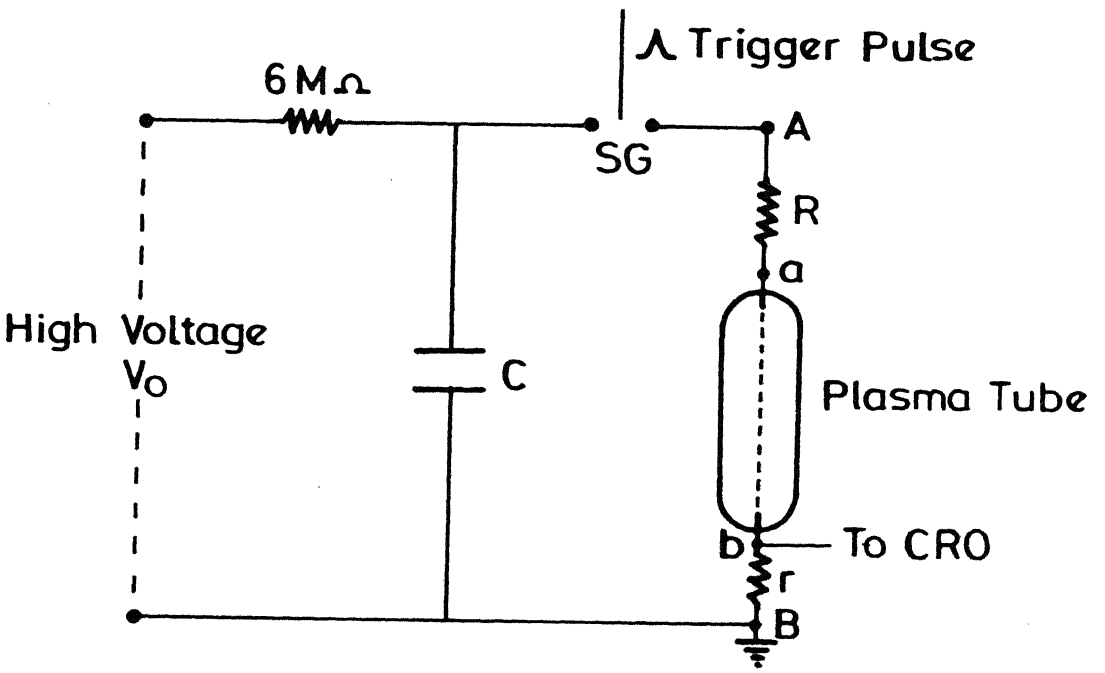

Fig. 3 RC CIRCUIT

capacitance were used, i 0.0091 μF, and ii 0.028 μF (ceramic capacitor, 30 KV). Below 0.0091 μF, we were not able to observe any laser action.

ii LC Circuit. A seven stage LC circuuit shown in Fig 4 was used, to get nearly flat top current pulse. Each inductor consisted of 25 windings of copper wire wound on a mylor cylinder of 4 cm diameter, the inductance as measured with bridge circuit was 14 μH. The value of each capacitance used was 4000 pF. The current pulse width being given by $2\pi\sqrt{(LC)}$ [68].

The spark gap was triggered with a 15 KV trigger pulse coming from a trigger transformer (home made). Trigger circuit used is shown in Fig 5. The trigger circuit can be operated in mannual or auto mode with a maximum repitition rate of 33 pps. A pulse of 300 V from the circuit was applied to the primary of the trigger transformer. A synchronizing pulse is taken out at S (Fig 5) through an isolation stage to trigger the detection system. During the experiment, the system was usually operated at 3 pps.

The discharge current was measured with a low inductance low resistance (90 mΩ) co-axial probe connected in series with the discharge tube as shown in Fig 3. The low resistance r was a small carbon rod enclosed in a brass capsule. One end of the carbon rod was connected to the enclosing capsule and was grounded and other end was connected to the discharge tube as shown in figure. Resistance R connected in series with the discharge tube was used to control the discharge current. The

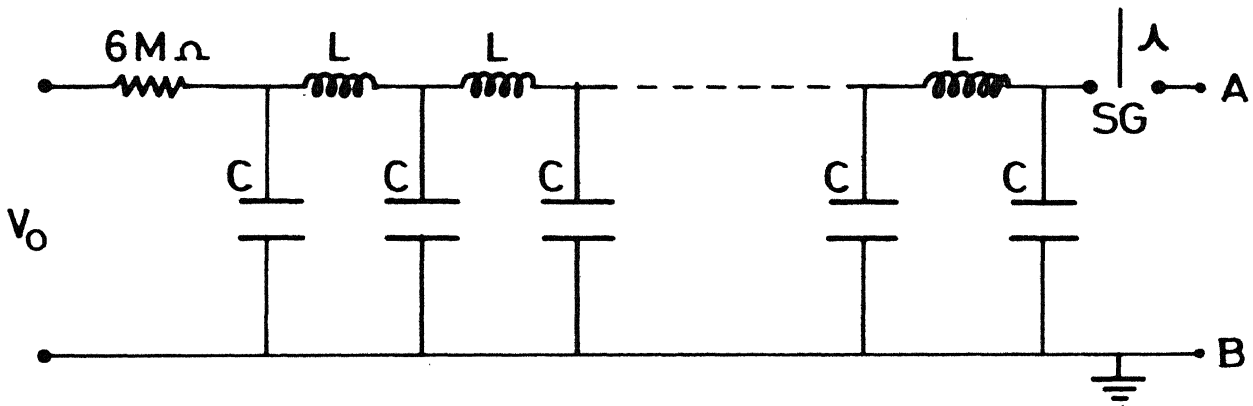

L = 14 μH
C = 4000 pF

Fig. 4 LC circuit

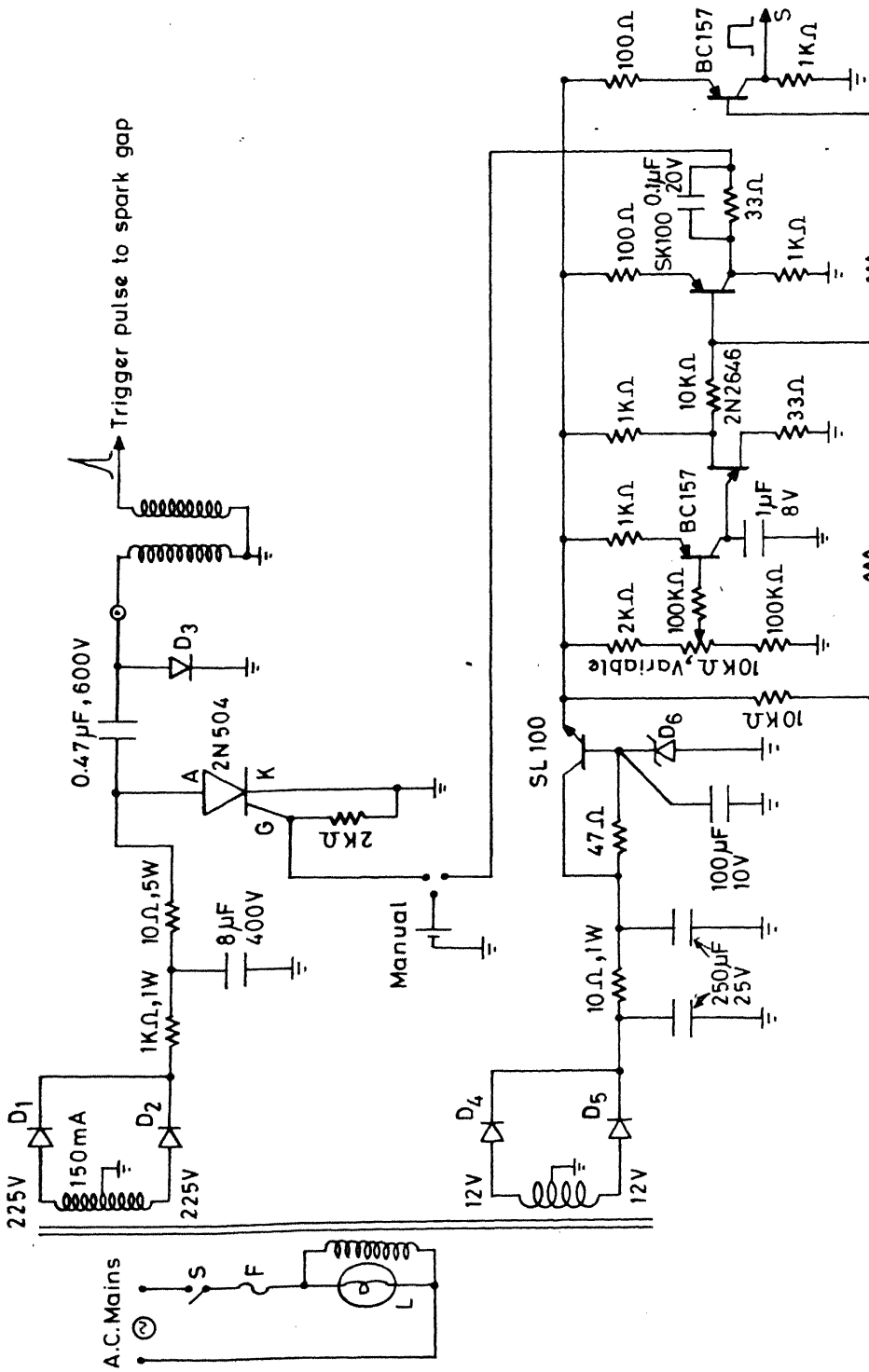

Fig. 5 Triggering circuit

voltage V was measured across the terminals A and B (Fig 3) using a high voltage 30 KV probe (1:1000). Fig 6 shows the linear variation of voltage V measured across A and B with respect to voltage V_o from the high voltage power supply for R = 150Ω. The typical voltage pulse and current pulse obtained with RC and LC circuits used are shown in Fig 7 for R = 0Ω, 50Ω and 250Ω. The variation of peak current I with the resistance R for RC and LC circuit is shown in Fig 8 for 40 and 70 plasma segements. In the following chapters the results are discussed in terms of value of R. Low resistance R implies high current and vice-versa. Fig 9 shows the variation of voltage V with the resistance R.

The resonator cavity was formed with two meter radius of curvature dielectric coated mirrors. For 1.65 μm transition, we used mirrors with high reflectivity from 1.35 μm to 1.53 μm, Optics for Research (USA) and for 1.43 μm transition mirrors from Tech Optics (U K) were used. To observe visible transitions at 533.7 nm and 537.8 nm, high reflectivity broad band mirrors (HR 488 nm to 515 μm, Tech Optics, UK) usually used with Argon ion laser were used.

Laser output from one of the mirrors was focussed on to the entrance slit of 0.32m monochromator with a lens of 10 cm focal length as shown in Fig 2. Grating with 600 grooves/mm and 1200 grooves/mm were used in monochromator for IR and visible radiation respectively. The output from the monochromator was detected with an optical detector. IR radiation was detected with a Judson's Ge detector. The detector was used in zero

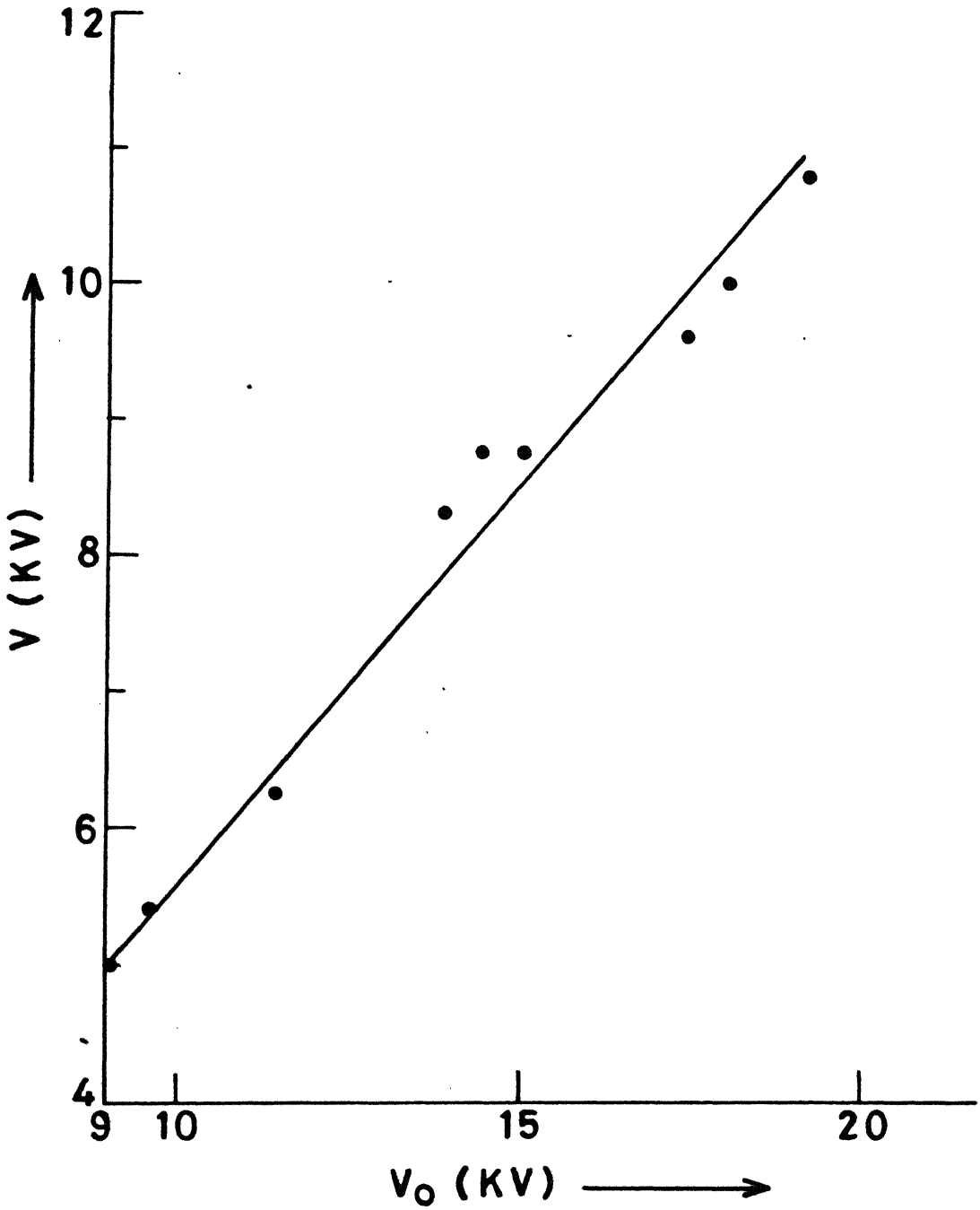

Fig. 6 Plot of V vs V_o for R = 150 Ω.

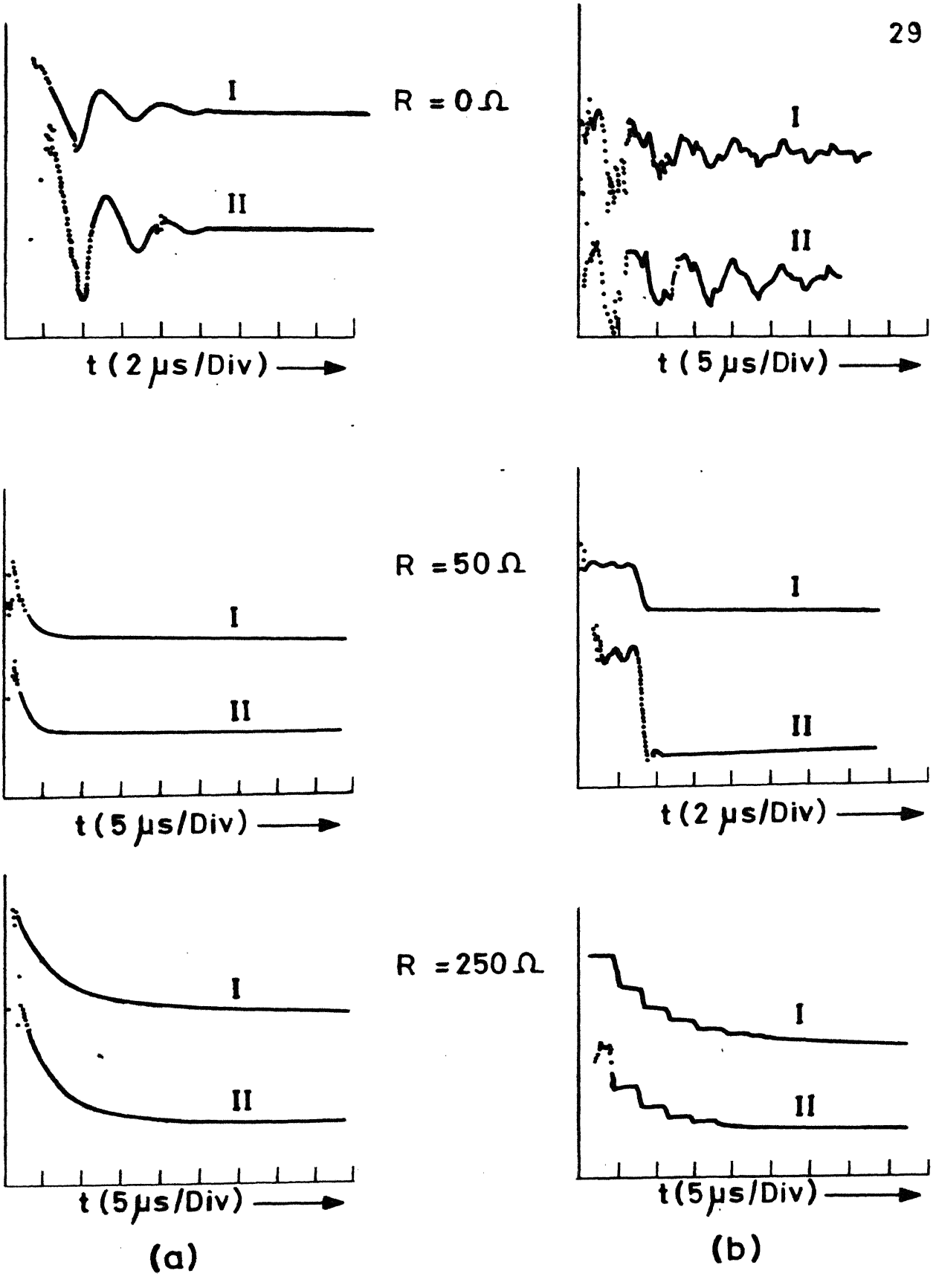

Fig. 7 Oscilloscope trace of
I – Voltage pulse
II – Current pulse

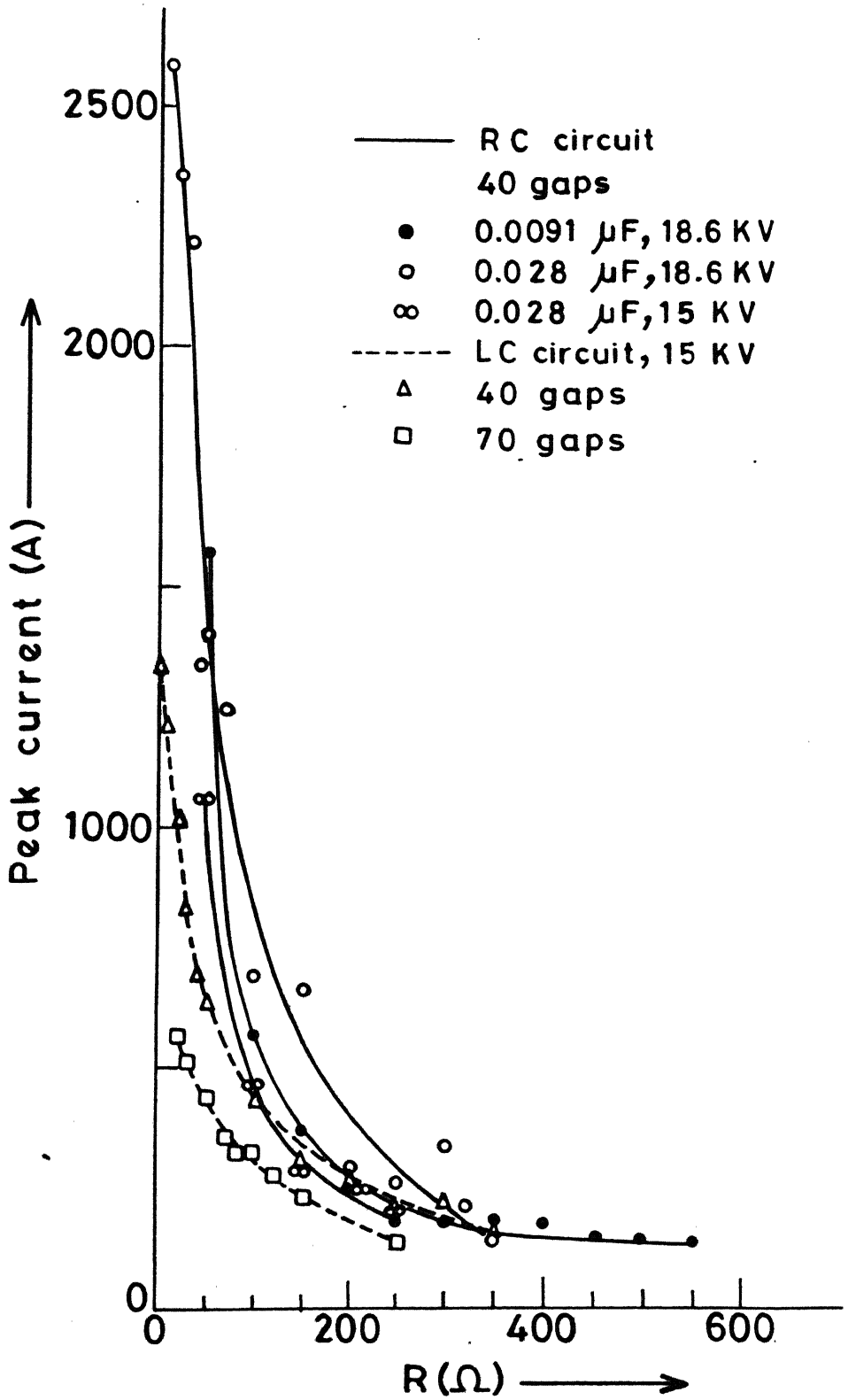

Fig. 8 Variation of peak current I with resistance R.

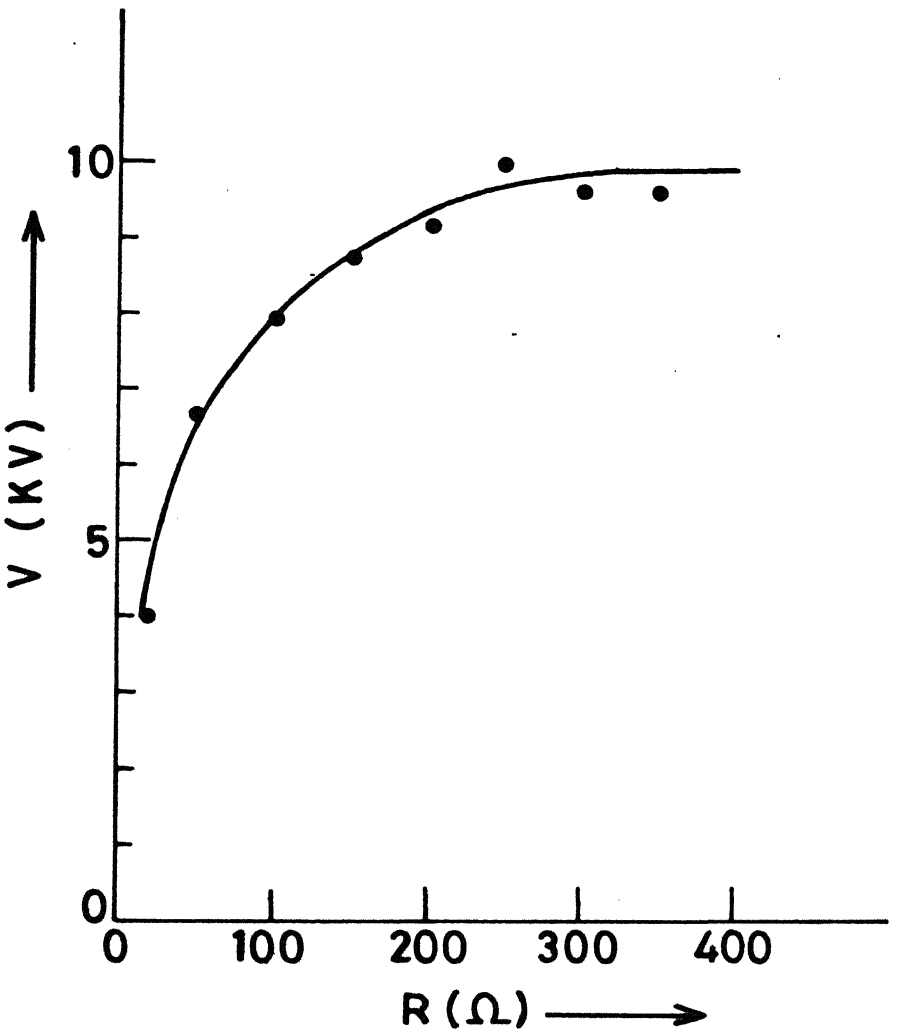

Fig. 9 Variation of peak voltage V with resistance R .

bias mode. The amplifier circuit, current to voltage conversion configuration is shown in Fig 10. For visible radiation, a photomultiplier tube (Hamamatsu R 446) with 50Ω termination was used to monitor the output. Output from either detector is displayed on the oscilloscope (100 MHz Iwatsu TS 8123) and fed on to the boxcar averager (SRS 250) as shown in Fig 2. Boxcar was triggered externally with synchronizing pulse from trigger circuit at S (Fig 5). Synchronizing pulse at S was cleaned by feeding the pulse through a two stage emitter follower circuit before applying it to boxcar averager. Emitter follower circuit is shown in Fig 11. Boxcar averager was operated in scanning mode with settings; gate width 9 μsec, scan width 200 μsec for IR laser. Corresponding values for visible laser were; gate width 900 nsec and scan width 15 μsec. Depending on the appearance of laser pulse, initial delay was adjusted. Averaging was done over 10 samples. The average output from the boxcar averager was recorded on the strip chart recorder.

We tried to scan the radial profile of IR laser. For scanning the radial profile, IR radiation is directly allowed to fall on to the detector. Neutral density filters were used in front of the detector to protect it from saturation. The detector was placed at a distance of 25 cm from the output mirror. Detector has an active area of diameter 1 mm. It was moved in steps of 1 mm to scan the radial profile.

Small signal gain was measured by inserting a variable loss

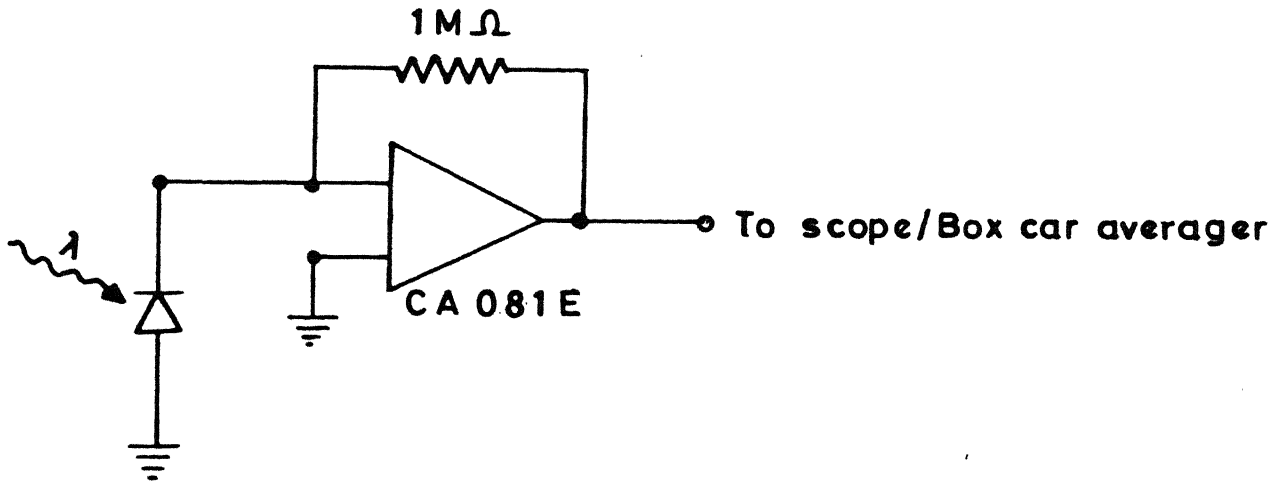

Fig.10 Zero bias circuit for Ge detector

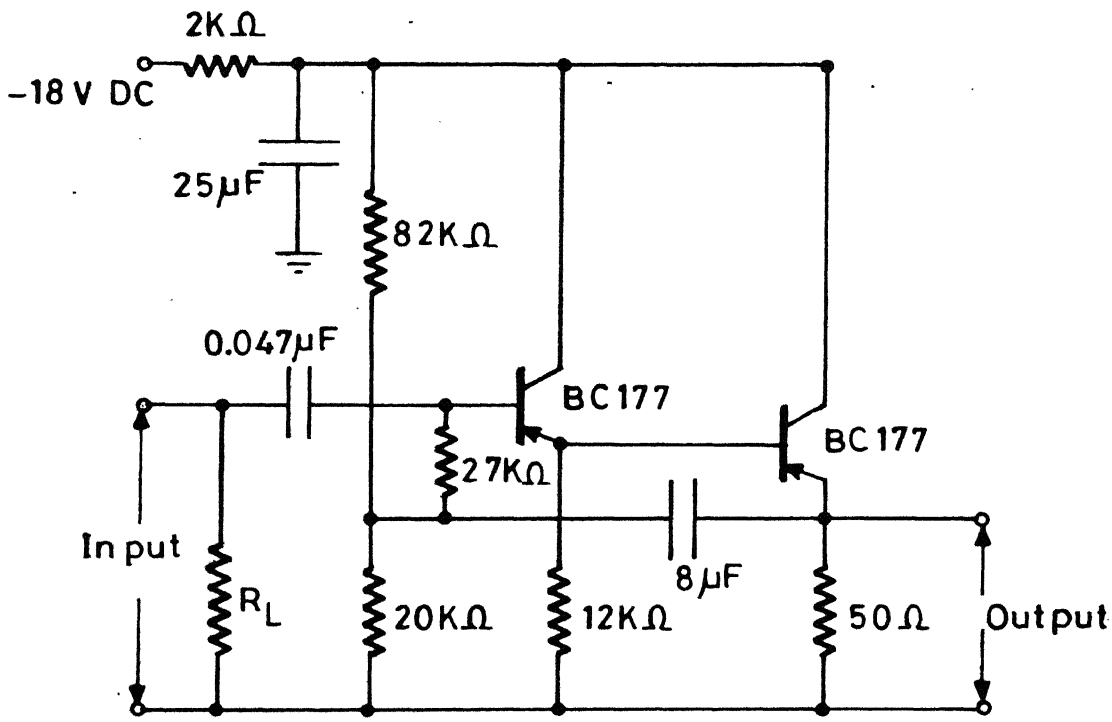

Fig. 11 Emitter follower circuit

into the cavity so that total loss into the cavity just balances the gain available in the medium. The small signal gain being given by [30]

$$G = \frac{1}{l} \ln \left[\frac{1}{\sqrt{(R_1 R_2)}\ T_B^2\ (1-L)} \right] \qquad 16$$

where, G is the small signal gain coefficient, l is the length of the active medium, R_1, R_2 are the reflectivities of the mirrors used, T_B is the transmission through each window of the discharge tube and L is the variable loss introduced into the cavity to achieve the threshold oscillation conditions. Gain measurements were made for 40 and 70 plasma segments with cavity length equal to 120 cm and 170 cm respectively. A pair of Brewster angle plates was introduced into the cavity [69]. Brewster plates were initially aligned with respect to the Brewster windows of the plasma tube. A known amount of loss was introduced into the cavity by rotating the plate about the resonator axis. If ϕ is the angle by which the plates are rotated to achieve the threshold condition, the gain expression in eq 16 can be rewritten as

$$G = \frac{1}{l} \ln \left[\frac{1}{\sqrt{(R_1 R_2)}\ T_B^2\ \cos^2\phi} \right] \qquad 17$$

The laser output was monitored with the angle of rotation of the plates till laser oscillations just stop.

To estimate temperature of plasma, visible cadmium spectrum

was recorded in presence of helium gas [70]. Single plasma segment was used for recording spectrum. The plasma radiation was focussed on to the entrance slit of the monochromator. Fig 12 shows the cadmium spectrum at P_{He} = 5 Torr. Based on earlier literature [71-73] Cd I and Cd II transitions were identified [70].

Assuming that plasma is in local thermodynamic equilibrium, an estimate of temperature was made by taking the ratio of intensity of two spectral lines and using the relation

$$kT_e = \frac{E'-E}{\ln(I\,\lambda\,g'A'/I'\,\lambda'\,gA)}$$

where E and E′ are the excitation energy of the levels, I's are intensity, g, A and λ are the respective statistical weight, transition probability and wavelength of transition under consideration. The slope of the curve (E′-E) against $\ln(I\,\lambda\,g'A'/I'\,\lambda'\,gA)$ gives temperature. The temperature lies in the range 0.5eV $\leq T_e \leq$ 1.0 eV for Cd I and 1.0 $\leq T_e \leq$ 2.0 eV for Cd II. It agrees well with the earlier report [74].

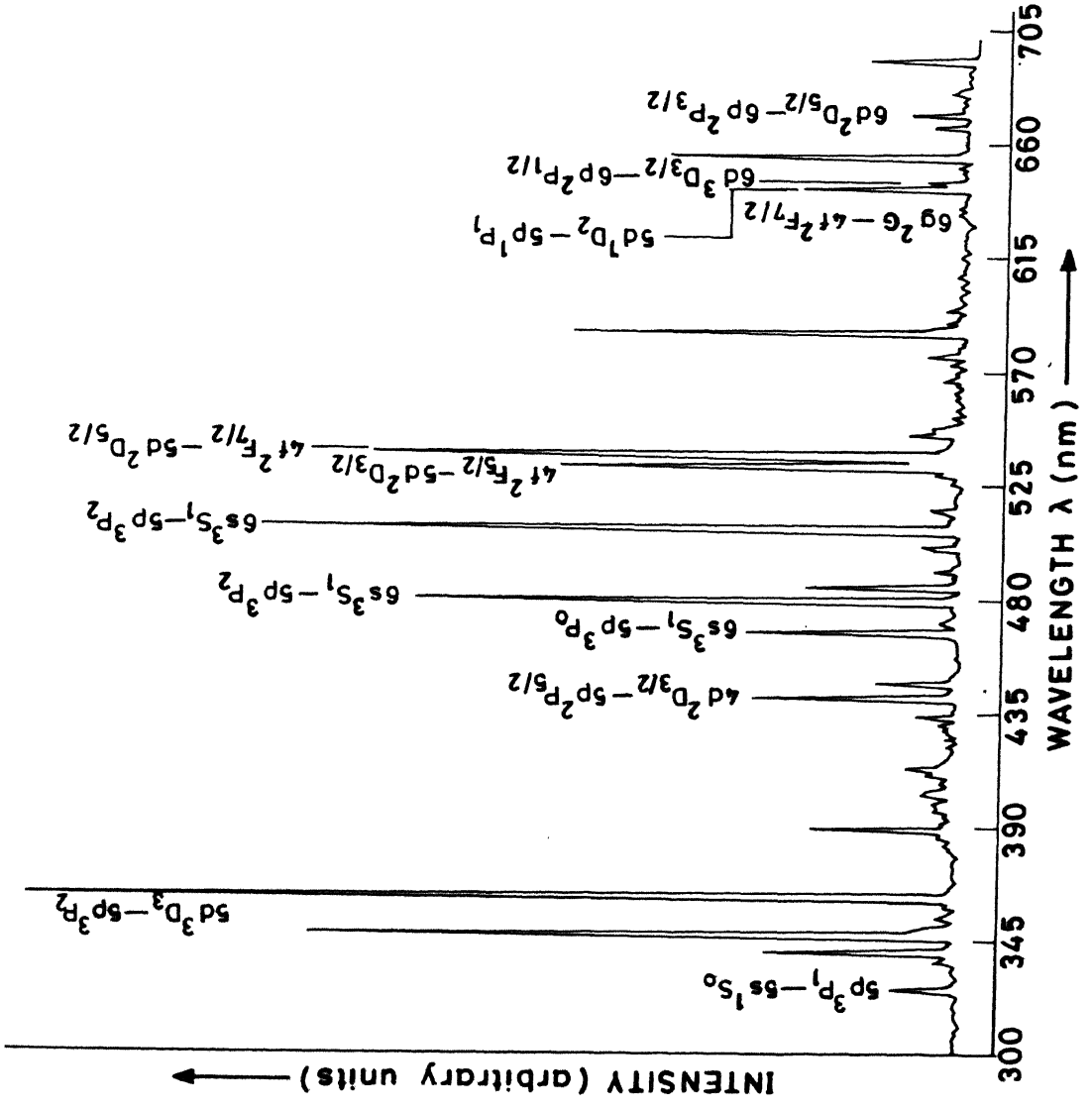

Fig. 12 Visible spectrum of cadmium.

Chapter 3

CHARACTERISTICS OF PULSED IR (Cd I) LASER

Introduction

The first observation of laser action in Cd at 1.65 μm and 1.43 μm transitions in pulsed mode was reported [75] in 1972. Based on recombination scheme, the laser action in cadmium on the above transitions was reported by Wood et al [24, 61]. They used continuously flowing helium as a buffer gas. Recently Rocca et al [28] have reported studies on the Cd I transitions in an e-beam generated plasma. However, there has been no report on the performance characteristics of cadmium plasma recombination laser. A detailed study was undertaken for cadmium plasma recombination laser based on SPER mechanism. Laser oscillations on $6p\ ^3P_2 - 6s\ ^3S_1$ at 1.40 μm, $6p\ ^3P_1 - 6s\ ^3S_1$ at 1.43 μm and $4f\ ^3F_4 - 5d\ ^3D_3$ at 1.65 μm transitions of Cd I using SPER configuration in a sealed discharge tube are reported for the first time [63]. Unlike conventional metal vapor lasers [37-41], the system developed does not require any additional heating arrangement to produce vapors of the metal. Details of the experimental set up used are given in Chapter 2. A schematic layout is shown in Fig 2. The active medium consisted of a large number of (10mmx2mmx1mm) strips of cadmium metal (Nuclear Fuel Complex, Hyderabad) positioned end to end on a glass substrate with a spacing of 1 mm between the adjacent strips. End strips

were used for applying high voltage, high current pulse. The resonator cavity was formed by using two meter radius of curvature dielectric coated mirrors. Two types of excitation circuits were used i RC circuit, a simple capacitor discharge circuit, and ii LC circuit. Circuits and typical current and voltage pulses are shown in Figs 3, 4 and 7 respectively. Laser Radiation was focussed on to the entrance slit of 0.32 m monochromator and was detected with Ge detector operated in zero bias mode. The biasing circuit is shown in Fig 10. Output of the detector was fed to the oscilloscope (Iwatsu TS 8123) and boxcar averager (SRS 250) and was recorded on strip chart recorder.

We give below the performance characteristics of 1.65 μm ($4f\ ^3F_4 - 5d\ ^3D_3$) and 1.43 μm ($6p\ ^3P_1 - 6s\ ^3S_1$) transitions of Cd I over a range of discharge parameters, resonator axis in the presence of low pressure helium gas.

Results and Discussions

a Resonator Axis

In our configuration we could observe laser action at as close as 3 mm and as far away as 14 mm parallel to and away from the row of cadmium strips for all the transitions viz; $6p\ ^3P_2 - 6s\ ^3S_1$, $6p\ ^3P_1 - 6s\ ^3S_1$ and $4f\ ^3F_4 - 5s\ ^3D_3$. Fig 13 shows the variation of peak laser output power P_o in terms of detector output voltage for 1.65 μm transiton with the resonator axis. The optimum value of resonator axis was found to be around 8 mm away from and parallel to the row of the cadmium strips. All the

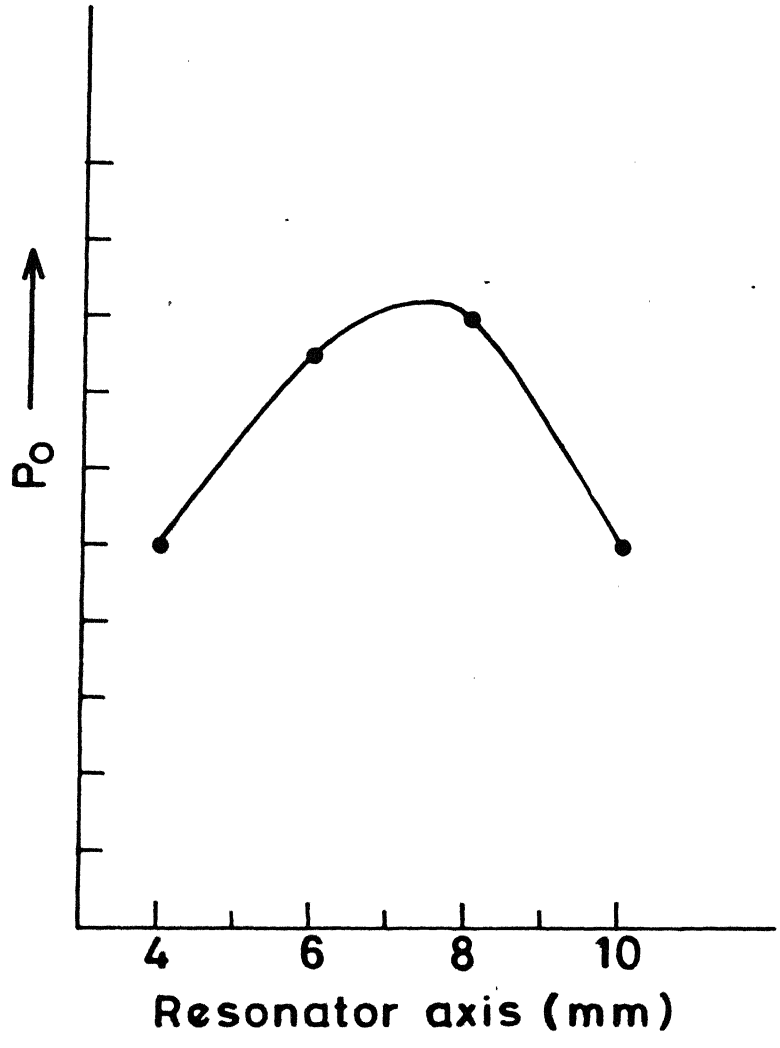

Fig. 13 Variation of the peak laser output power P_o as a function of resonator axes at $V_o = 12\,KV$, $C = 0.028\,\mu F$, $R = 200\,\Omega$, $P_{He} = 8\,Torr$.

characteristics of laser were studied at this optimum position of the resonator axis.

b Effect of Shape of Current Pulse and Current on Stimulated Emission

Stimulated emission was observed in the afterglow region. Fig 14 shows the delay between the spontaneous emission and the stimulated emission for 1.65 μm transition for RC circuit. We have observed the delay between the current pulse and the laser pulse as much as 170 μsec. Long delay confirms that the laser action occurs in the afterglow region of the plasma. Delay increases as the peak current increases (R decreases). The variation of delay of the laser pulse, τ_d with R is shown in Fig 15. For lower values of dumped energy ($\frac{1}{2}CV^2$), τ_d is also low. Towards high value of resistance (R>200Ω), delay increases slightly with resistance. This could be attributed to excitation of lower laser level at low current. Laser action was also observed for low values of R (high current) with ringing frequency of 0.36 MHz in the current pulse. The long delay observed suggests that the shape of the current pulse should not be a critical parameter for observing infrared transitions in the configuration used. Experiments performed using simple capacitor discharge circuit and LC circuit showed similar behaviour.

The variation of peak laser output power P_o for 40 gaps with the resistance R for 1.65 μm and 1.43 μm transitions is shown in Figs 16 and 17 respectively. Fig 18 shows the variation for both

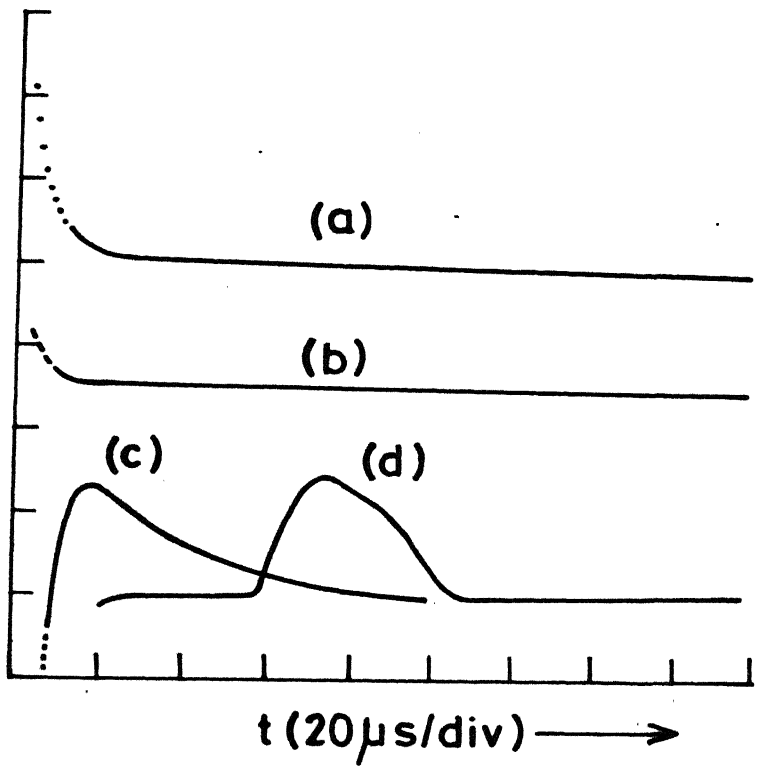

Fig. 14 Oscilloscope trace of (a) Voltage pulse
(b) Current pulse
(c) Spontaneous emission
(d) Stimulated emission

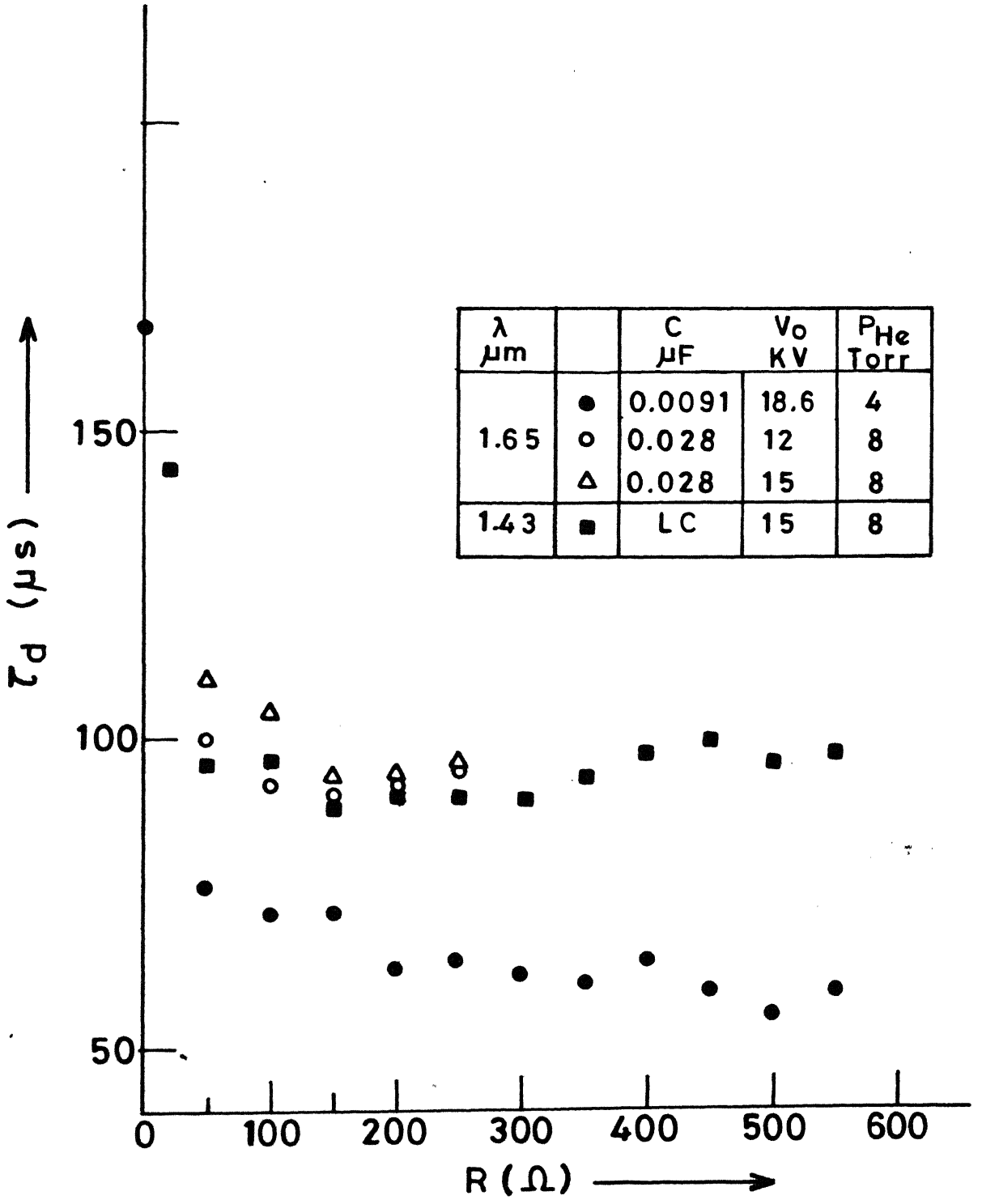

Fig. 15 Variation of delay τ_d of appearance of peak of laser pulse with resistance R.

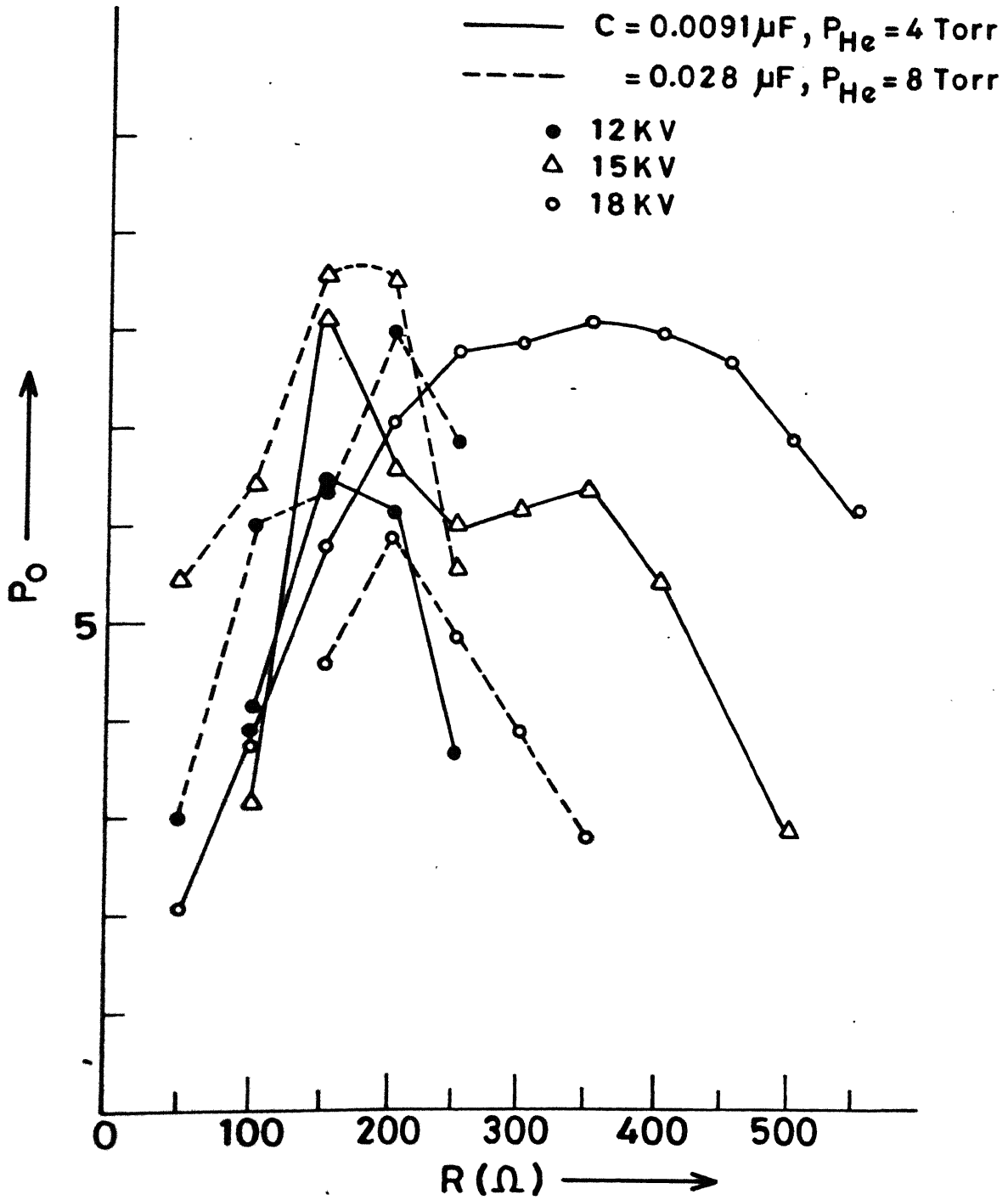

Fig. 16 Dependence of peak laser output power P_O on resistance R.

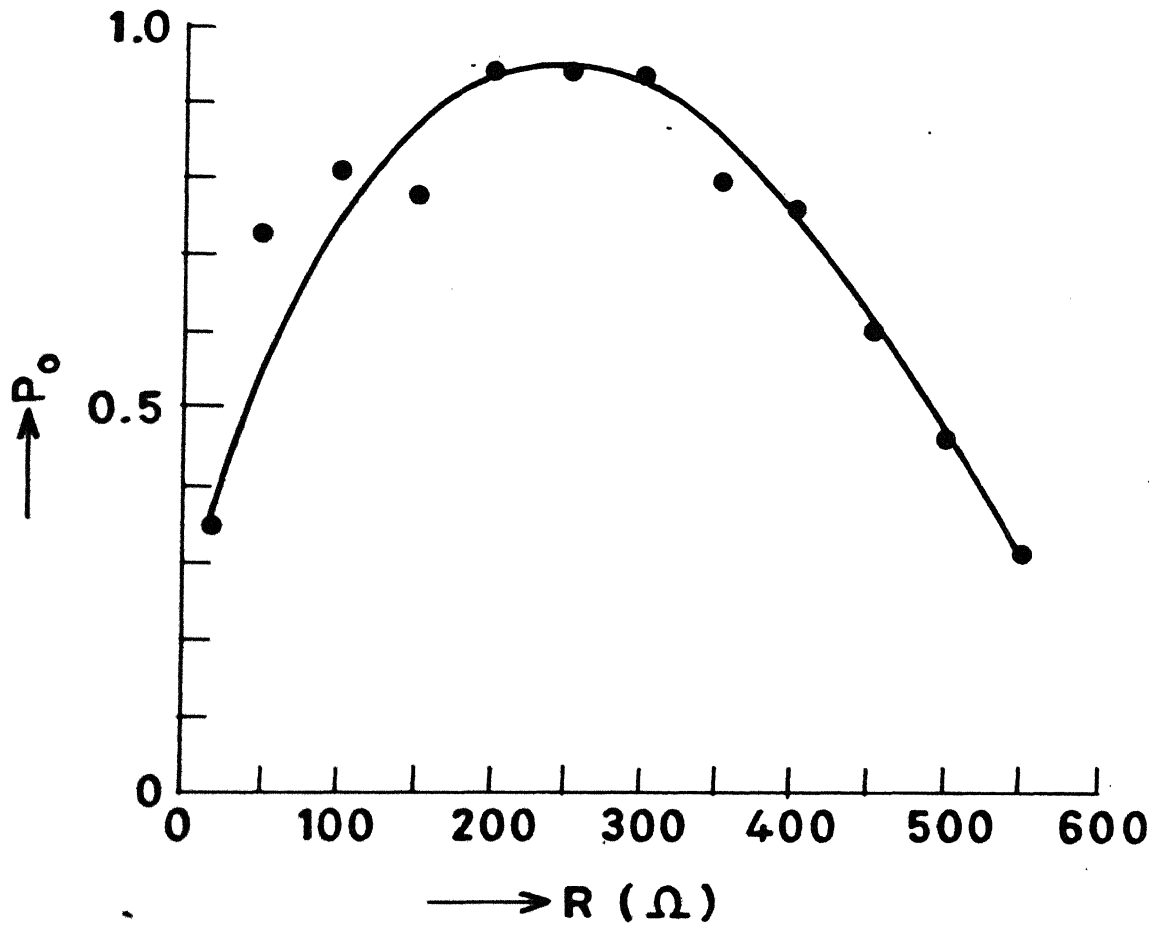

Fig. 17 Dependence of peak laser output power P_o on resistance R at $P_{He} = 8$ Torr, $V_o = 15$ KV for LC circuit.

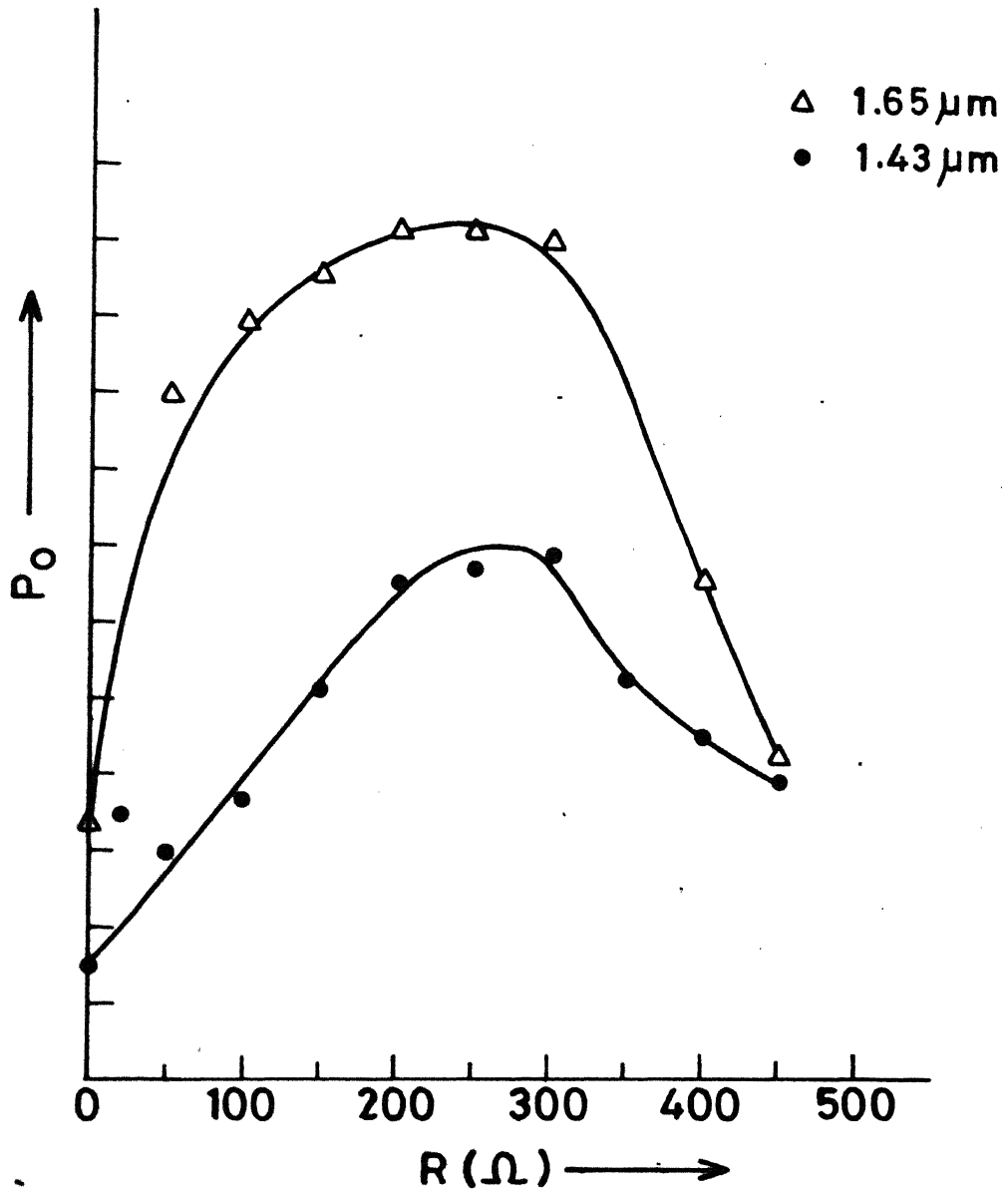

Fig. 18 Dependence of peak laser output power on resistance at optimum He pressures for LC circuit at $V_0 = 15$ KV.

the transitions for 70 segements. Initially P_o increases with the increase in current, reaches an optimum value and then decreases with further increase in current. At large currents, though the higher levels are filled very effectively by recombination pumping, simultaneously, collisional processes start dominating at higher electron density. Therefore, electronic de-excitation of upper level is much faster than those of lower ones. This process effectively decreases the net population inversion and hence the laser output power. Fig 19 shows the variation of P_o with voltage V and current I for 1.65 μm transition for an LC circuit. At high current, the laser pulse is usually broad. It may be due to high temperature and high electron density of the plasma at high current. Laser pulse corresponding to 1.43 μm is broad (FWHM 52 μs) compared to that of 1.65 μm (FWHM 42 μs),as shown in Fig 20. We have also observed a multiple peak structure in the laser pulse which may be due to inhomogeneous expansion of plasma.

c Effect of Pressure of Background Gas

The role played by background gas in the recombination laser is two fold. When a high current, high voltage pulse is applied, it helps in creating a high concentration of the ions of the metal (lasing species). After the end of the current pulse, electrons cool very rapidly via collisions with buffer gas atoms and ions resulting in decrease in temperature. The process helps in populating the excited states (upper laser level) by strong

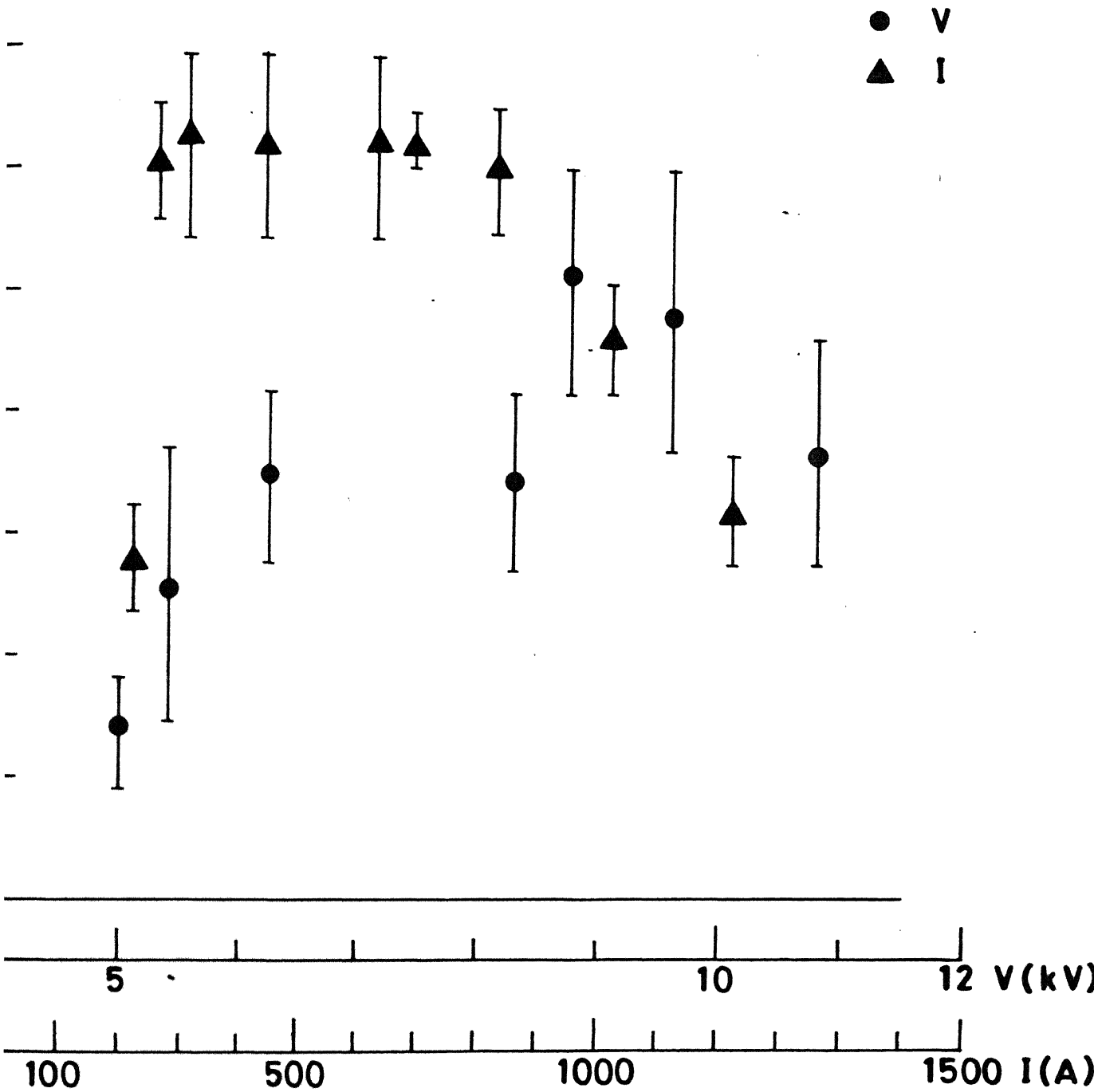

Fig.19 Variation of peak laser output power P_o at $P_{He} = 8$ Torr as a function of
(a) voltage V at $R = 150\ \Omega$
(b) current I

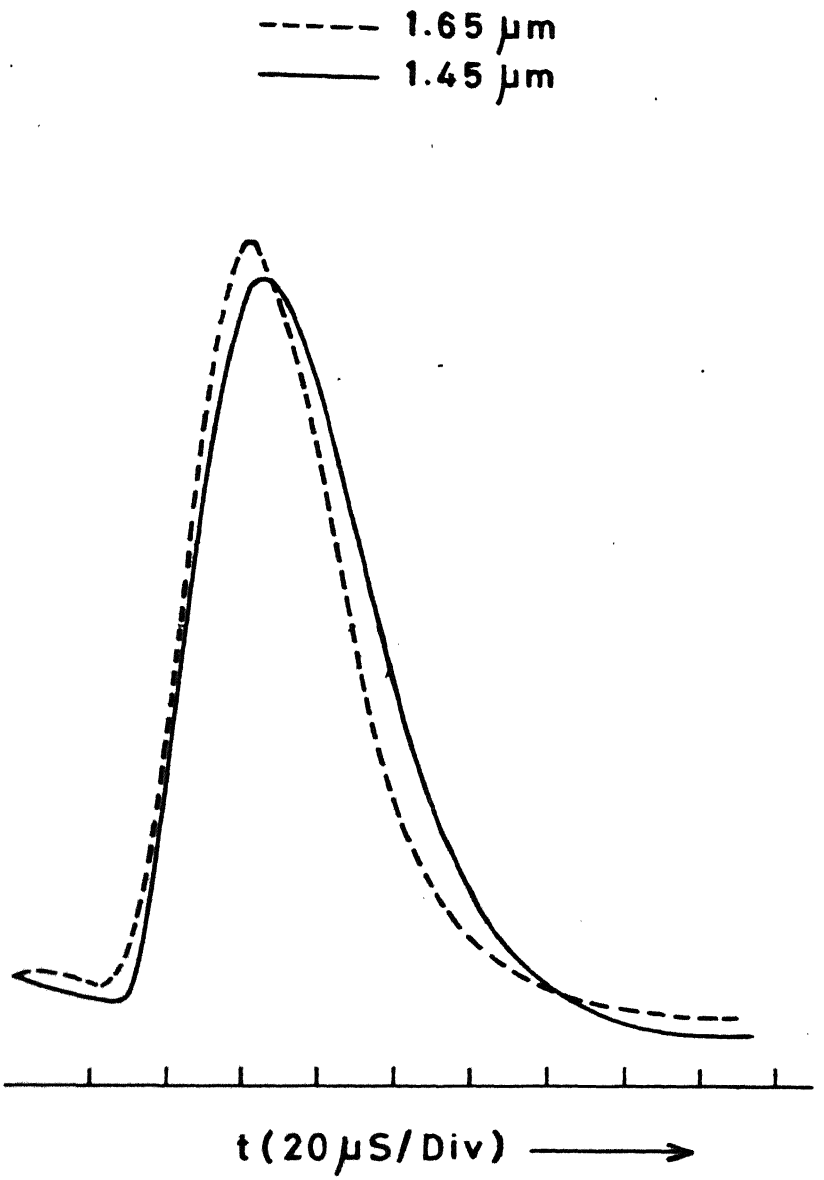

Fig. 20 Laser pulse corresponding to 1.65μm and 1.43μm transitions

recombination. Helium gas was used as background gas for most of the investigations. However, to see the effect of other background gases, we used neon, argon and mixture of He-Ne gases also. Figs 21 and 22 show the variation of peak laser output power P_o as a function of helium gas pressure for 1.65 μm and 1.43 μm transitions respectively. No laser oscillations were observed in vacuum (pressure $\leq 10^{-4}$ Torr) and upto 2 Torr of helium gas pressure. In vacuum the plasma expands freely, the electron density decreases faster than the electron temperature and hence the medium quickly deviates from the conditions of population inversion. However, in the presence of a background gas, the gain medium is confined to small region, providing sufficient plasma density. Cooling takes place via collisions with the background gas atoms resulting in population inversion. As is shown in Fig 21, laser action was observed at 3 Torr of helium gas pressure for C = 0.0091 μF and at 4 Torr for C = 0.028 μF. Laser output power increases with the increase of pressure, attaining a maximum value and then falls down with pressure. At very high pressure of background gas, cooling is very fast, the electrons come down via energy levels, cross the upper laser level resulting in populating the levels below the upper laser level Therefore, population inversion and hence the laser output will fall. For 1.65 μm transition at C = 0.0091 μF, the optimum value of helium pressure is 4 Torr and at C = 0.028 μF it is around 8 Torr. The optimum value of helium

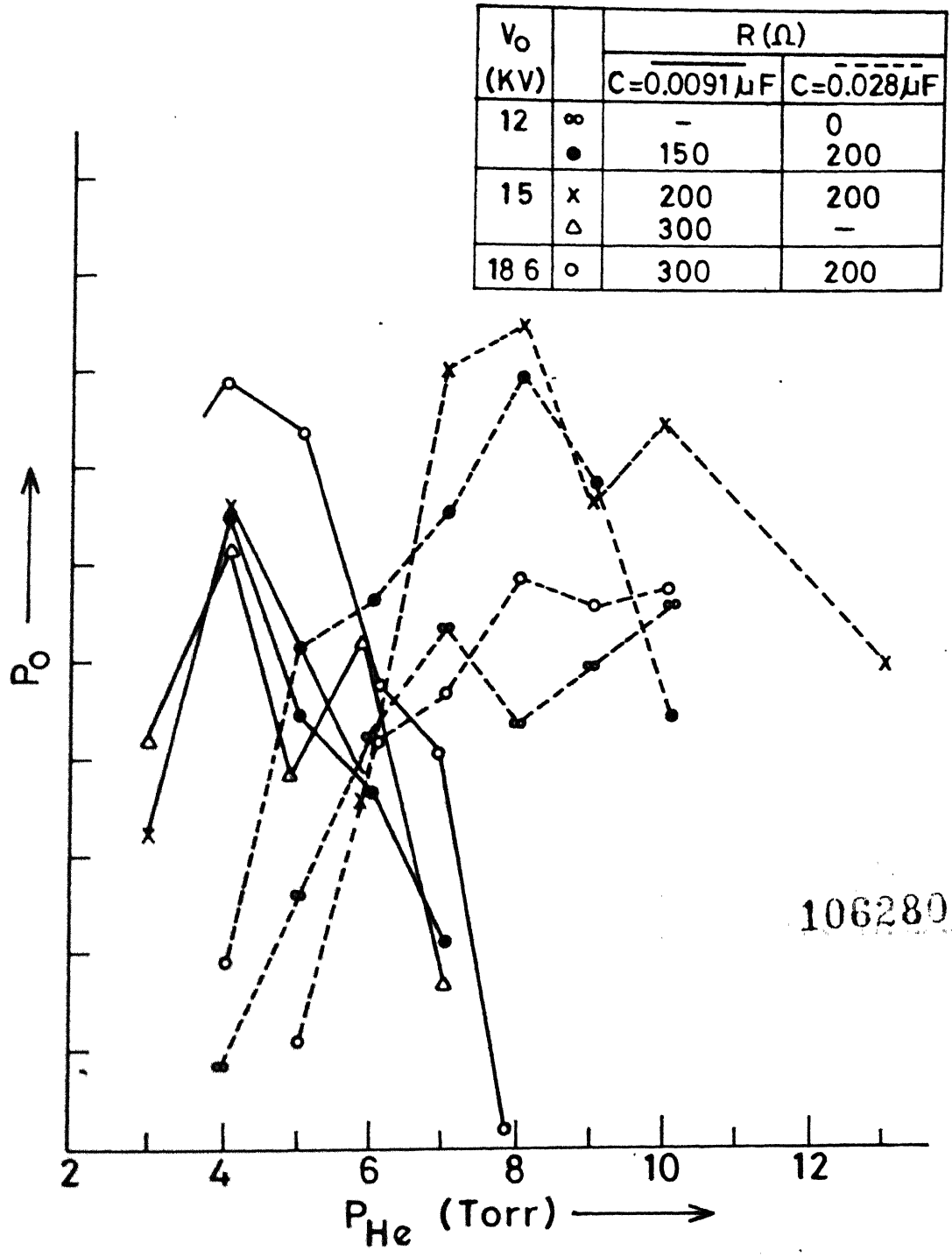

Fig. 21 Effect of pressure of helium gas on peak laser output power.

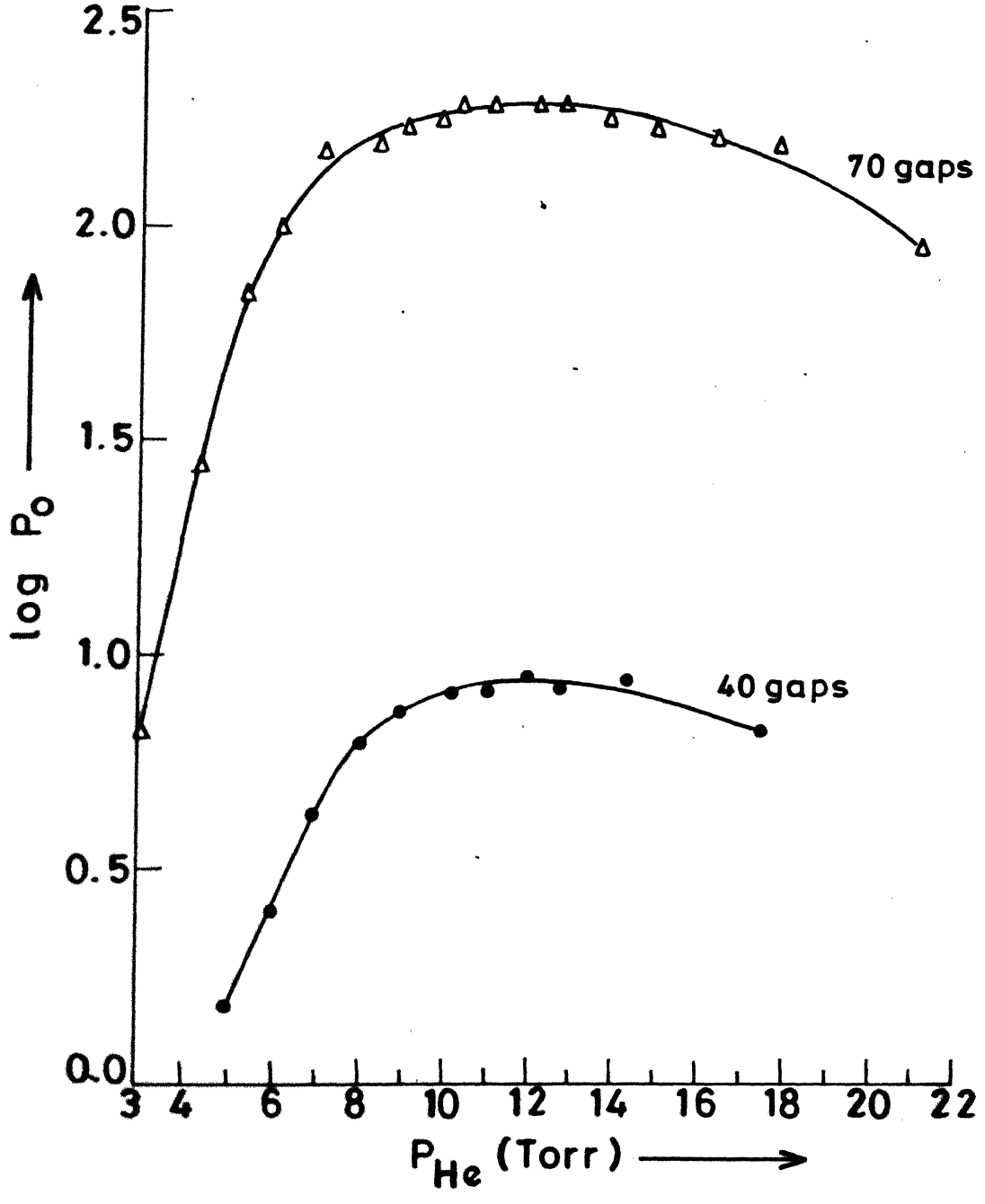

Fig. 22 Variation of peak laser output power with pressure of background gas He at $V_o = 15KV$ for LC circuit.

pressure for 1.43 μm transition is found to be higher (12-14 Torr) than that for 1.65 μm transition (8-9 Torr) for identical input energy. This difference can be explained with the help of the partial energy level diagram [71-73] of Cd I, as shown in Fig 23. Since the excitation energy for 1.43 μm transition (7.24 eV) is lower than that of 1.65 μm transition (8.13 eV), therefore, for the same input energy, former will require more electron cooling implying a high pressure of background gas to reach an optimum value of temperature and density for efficient recombination pumping.

Experiments were performed with other gases, Ne, Ar and mixtures of He and Ne also. No laser action was observed with Ar at any pressure. However, in the presence of neon gas at a pressure of 4-5 Torr the laser output was observed, though very small. Due to large pulse to pulse variation, it was difficult to do any systematic study. An extensive study was done with various ratios of mixtures of helium and neon gases. Fig 24 shows the variation of peak laser output power as a function of total background gas pressure for various proportions of He and Ne. It is observed that as the concentration of neon in the mixture increases laser output falls down and the total optimum pressure shifts towards the lower pressure side. Effect can be explained by considering the expression for electron cooling eq 9, it is inversely proportional to the atomic mass M_B of the background gas. Neon gas, being heavier than helium gas, the

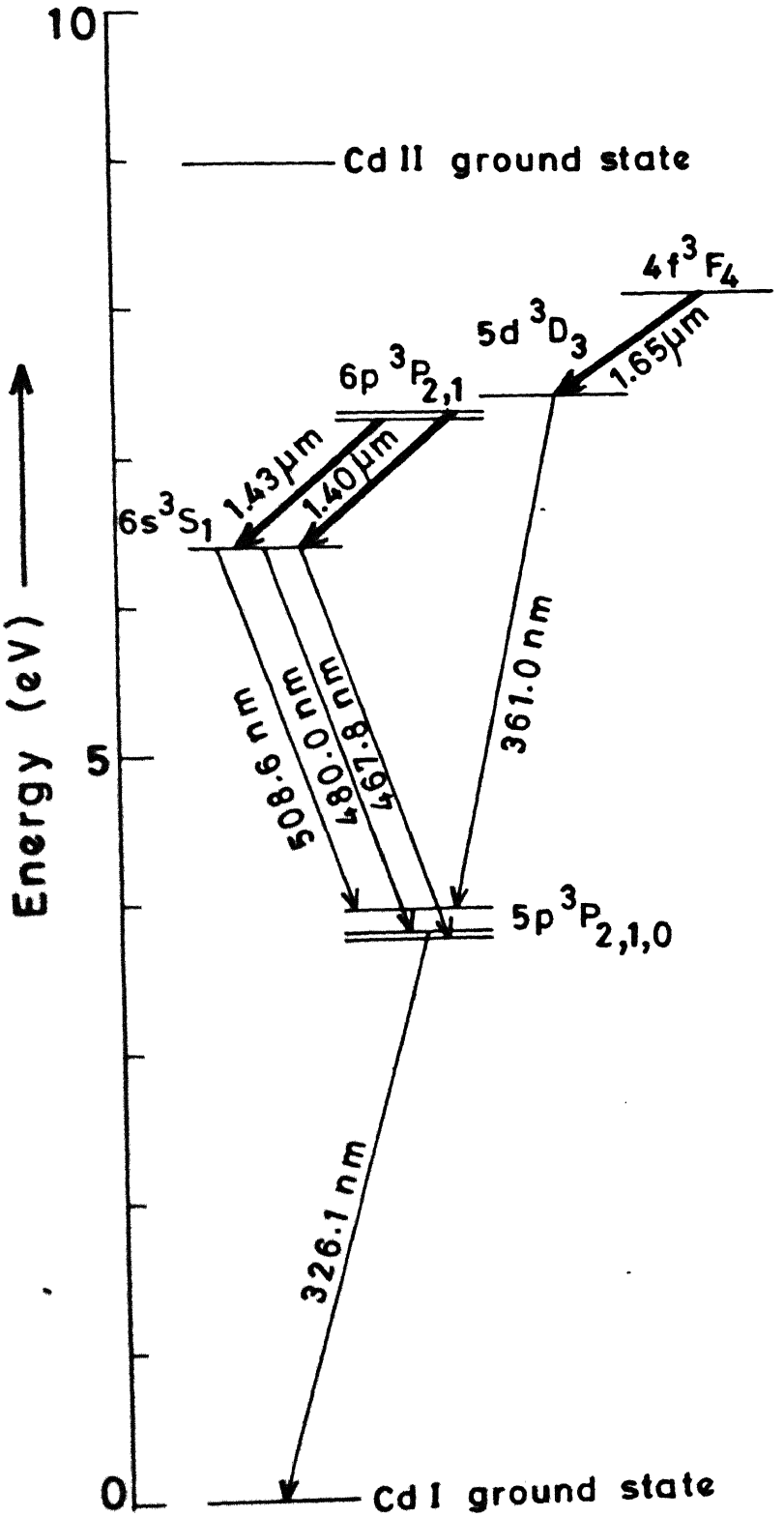

Fig. 23 Partial energy level diagram of CdI

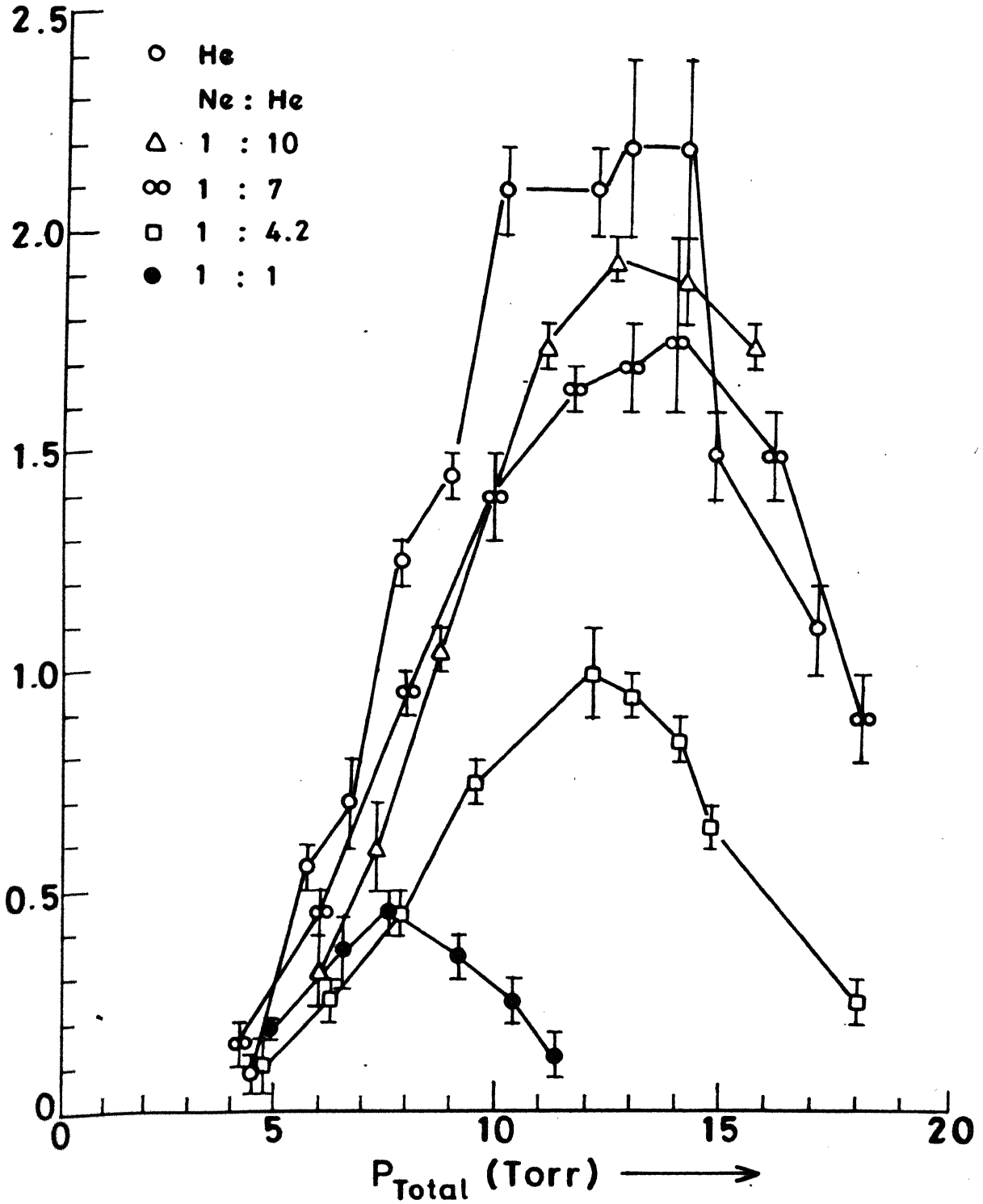

Fig. 24 Behavior of peak laser output power P_o with pressure of He-Ne gas mixture.

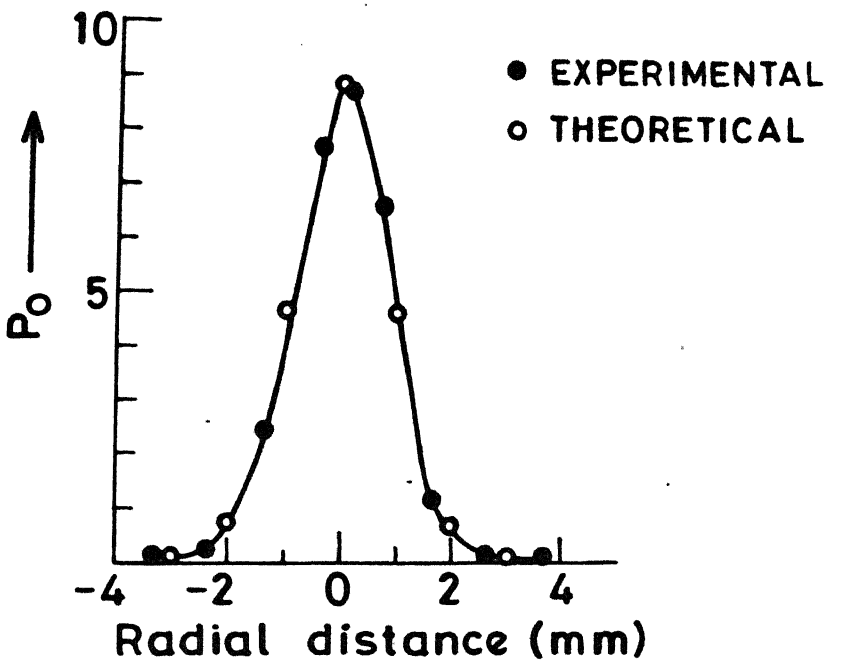

(a)

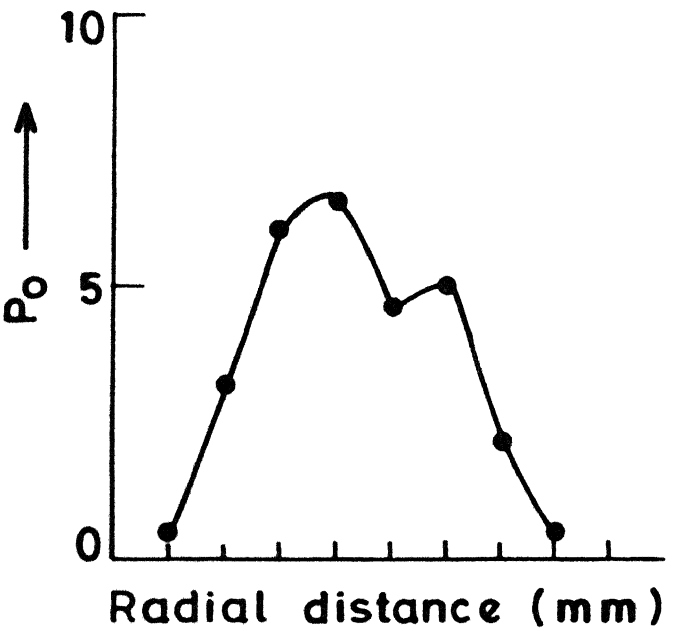

(b)

Fig. 25 Radial profile of laser output
(a) $V_o = 15$ KV, $C = 0.028\,\mu F$, $R = 200\,\Omega$, $P_{He} = 8$ Torr
(b) $V_o = 15$ KV, $C = 0.0091\,\mu F$, $R = 200\,\Omega$, $P_{He} = 4$ Torr.

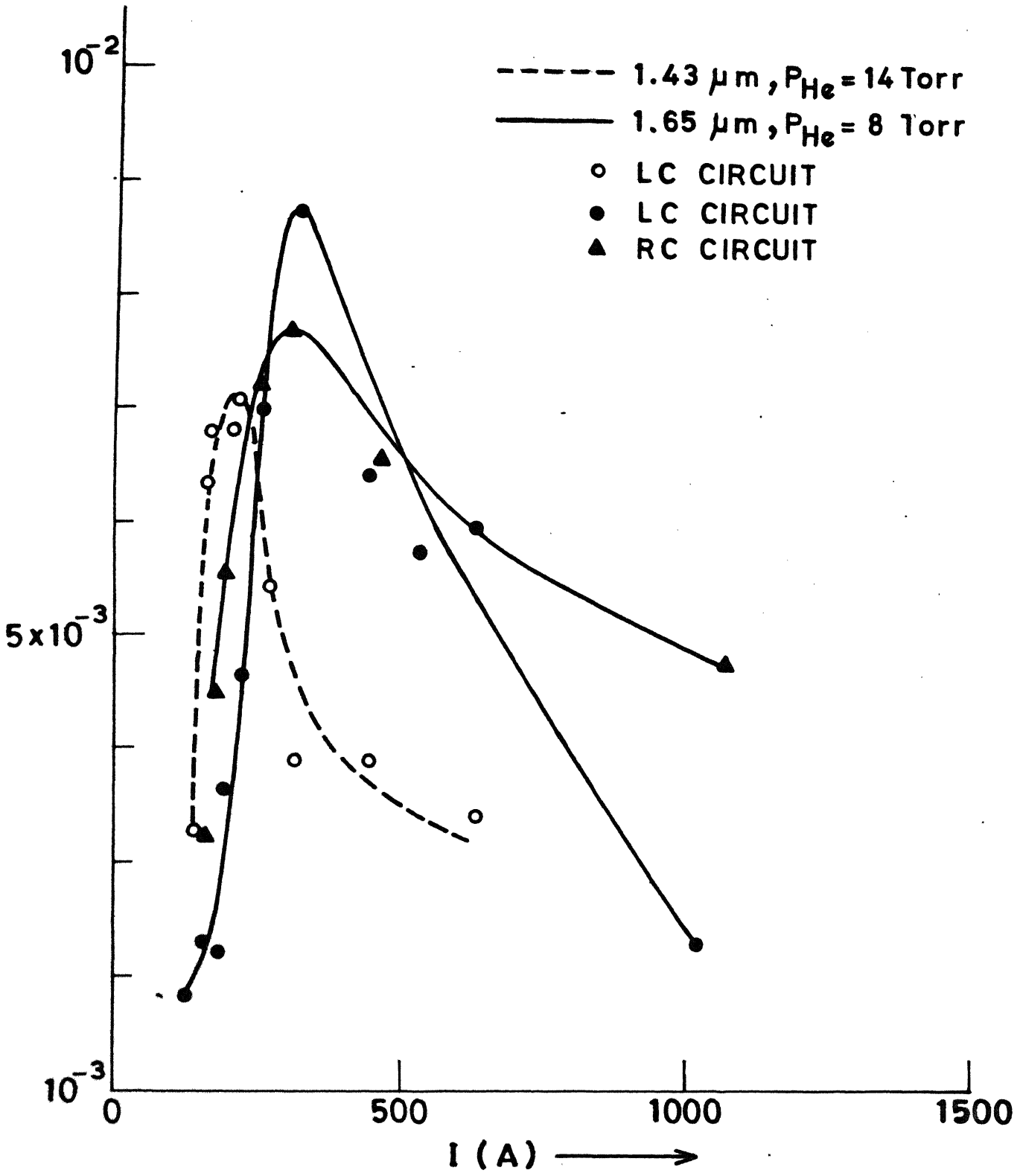

Fig. 26 Dependence of gain on current at $V_0 = 15$ KV.

The measured gain for RC circuit is found to be less compared to that of LC circuit. Hence, though the performance of a laser is similar for two shapes of current pulses used, we conclude that LC circuit is more efficient than that of simple capacitor discharge circuit. Fig 27 shows the variation of G with the helium gas pressure for 1.65 μm trasition. The maximum gain is obtained at a pressure of 8 Torr for 1.65 μm transition. The maximum gain estimated is 7.06×10^{-3} cm^{-1}, 8.73×10^{-3} cm^{-1} for 1.43 μm and for 1.65 μm transitions respectively.

To conclude, we have observed the pulsed laser operation at 1.40 μm ($6p\ ^3P_2 - 6s\ ^3S_1$) at 1.43 μm, ($6p\ ^3P_1 - 6s\ ^3S_1$) and at 1.65 μm ($4f\ ^3F_4 - 5d\ ^3D_3$) transitions of Cd I. Results of detailed studies of IR laser in Cd I at 1.65 μm and 1.43 μm transitions in SPER configuration in a sealed system are presented. Two types of excitation circuits a RC circuit, b LC circuit were used to create the cadmium plasma. A large delay, depending on the current is observed between the current pulse and the appearance of laser action. Laser output is dependent on the discharge current and the background gas pressure. We tried He, Ne, Ar and mixtures of He and Ne as buffer gases . Helium is found to be the best candidate for our configuration. The optimum pressure of helium gas for 1.43 μm is higher than that for 1.65 μm. Shape of the current pulse didn't appreciably effect the performance characteristics of laser; though LC circuit is more efficient. The effect of the increase of the

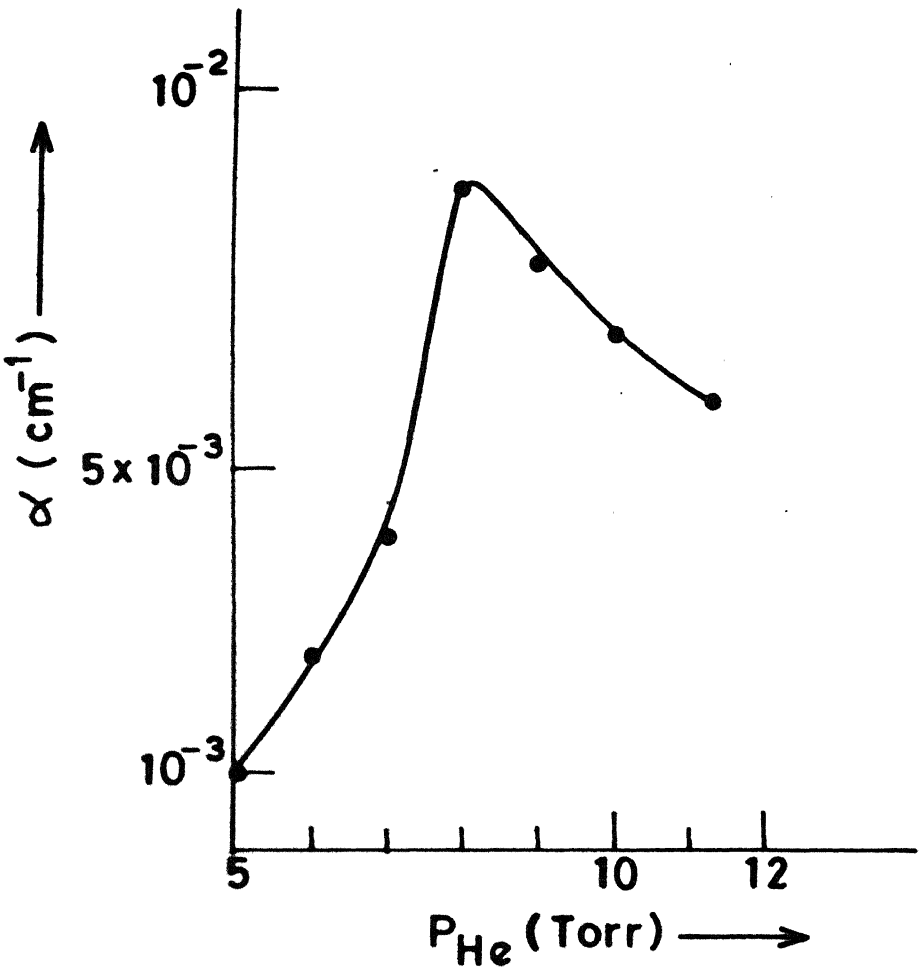

Fig. 27 Effect of pressure of background gas on gain at $V_0 = 15KV$, $R = 150\ \Omega$

length of the active medium by increasing number of plasma segments is reported. Measurements of small signal gain for both the transitions observed is reported. No significant variation was observed in the laser output for operating at 3 pulses per second for 48,000 pulses with one fill of helium.

Chapter 4

CHARACTERISTICS OF PULSED VISIBLE (Cd II) LASER

Introduction

First observation of laser action in Cd II at 533.7 nm and 537.8 nm transitions was reported in a hollow cathode [76-78] using transverse electric discharge. The excitation mechanism was based on the charge transfer collisions. The laser was observed in cw mode. Recently, oscillations on the above transitions have been observed based on recombination pumping mechanism [79] also. We reported [64] for the first time, the laser action on the above two transitions based on recombination scheme using helium as a buffer gas at low pressure of few Torr in a sealed discharge tube. The laser was observed in pulsed mode. We describe below the performance characteristics of the observed visible laser action in pulsed mode.

Experimental set up used has already been described in Chapter 3 and was similar to that used for IR laser. The laser cavity was formed by using two wide band dielectric coated mirrors (HR 480 nm to 514.5 nm, Tech Optics, UK), usually used with Argon ion laser, with 2 meter radius of curvature. Both types of excitation circuits, described in Chapter 2, were used. Helium was used as background gas. Laser radiation was focussed on to the entrance slit of 0.32 m monochromator and is detected with photomultiplier tube (Hamamatsu R 446, rise time 2.2 nsec). Photomultiplier tube signal was fed to the boxcar averager and

recorded on the chart recorder. Characteristics of laser at 537.8 nm ($4f\ ^2F_{7/2} - 5d\ ^2D_{5/2}$) transition of Cd II are given below.

Results and Discussions

We observed laser action at 533.7 nm ($4f\ ^2F_{5/2} - 5d\ ^2D_{3/2}$) and 537.8 nm ($4f\ ^2F_{7/2} - 5d\ ^2D_{5/2}$) transitions of Cd II. Laser action was observed from 3 to 14 mm away from the metal surface. The optimum value of resonator axis was found to be 8 mm away from metal surface, similar to that observed for IR transitions. All the characteristics presented below correspond to this optimum value of resonator axis.

a Effect of Length of Gain Medium

To see the effect on laser output with increasing the length of the active medium, we tried 10, 40 and 70 segments of cadmium plasma. In each case, the spacing between adjacent strips was kept constant. Dimensions of strips were also kept constant (10mmx2mmx1mm). However, the cavity length was varied,(75 cm, 112 cm and 135 cm) depending on numbers of plasma segments(10, 40 and 70 respectivey). On increasing the number of plasma segments to 70, one could easily see a green laser output on a white background. Fig 28 shows the variation of peak laser output power P_o with the number of plasma segments for the same energy dumped into the system. Each point on the curve corresponds to respective optimum value of helium pressure. Similar behaviour was observed for IR laser. Thus by increasing

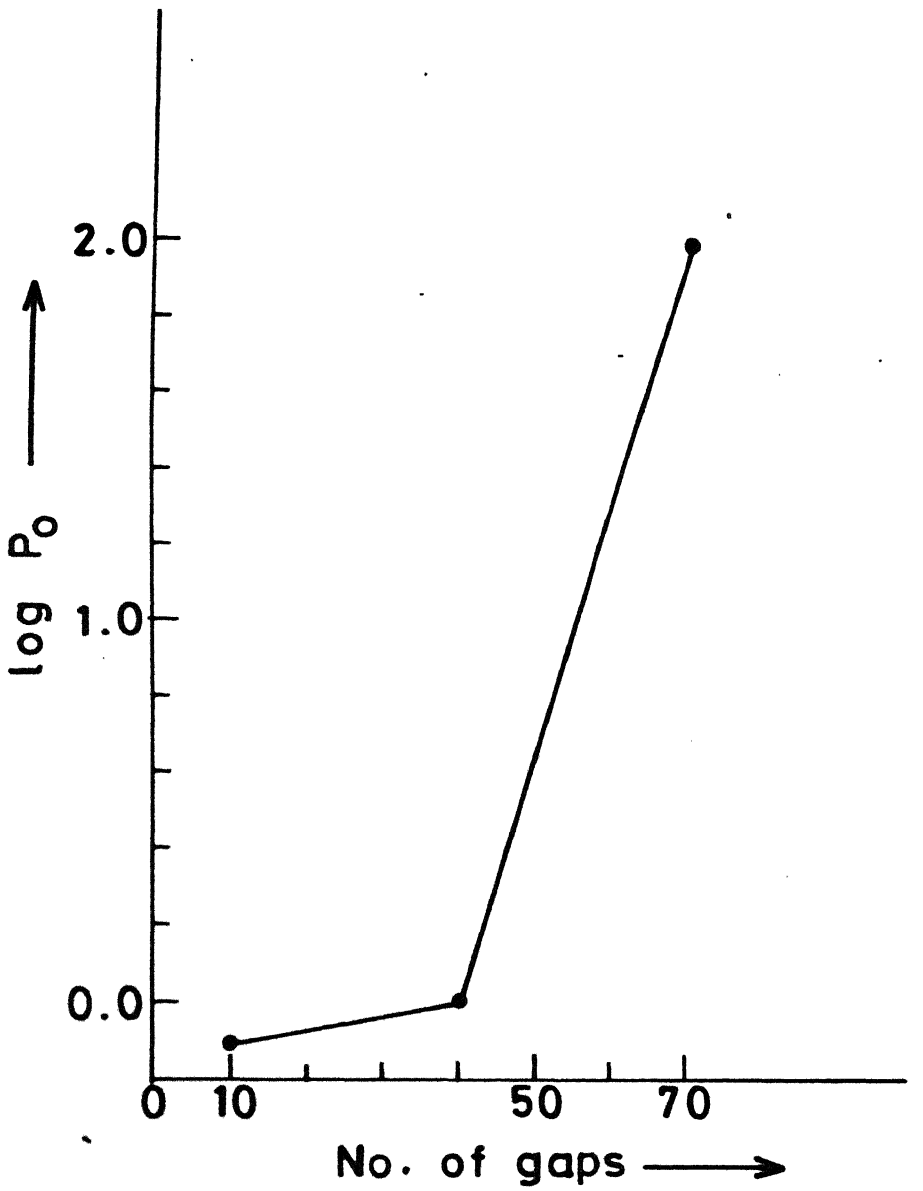

Fig. 28 Variation of peak laser output power P_o with number of plasma segments.

the number of plasma segments it should be possible to increase the laser output power.

b Effect of Shape of Current Pulse

Laser pulse is observed to be of 6 to 10 μs duration. Similar to IR laser, visible laser was also observed in afterglow region. However, the delay between the laser pulse and the current pulse observed was less than that observed for IR transitions. Maximum delay between the peak of the laser pulse and the current pulse is observed to be 30 μs. Fig 29 shows the laser pulse and the current pulse. Delay increases with current. Usually, we observed a double peak structured pulse. Double peak structure becomes more prominent as the number of segments increases. This may be due to inhomogeneous expansion of plasma or non uniform distribution of input energy for large number of segments. The variation of peak laser output power with resistance for an LC circuit for 70 segments is shown in Fig 30. Optimum value of current (R≈100Ω) for visible transition was higher than that for IR transitions. Transitions at 533.7 nm and 537.8 nm are obtained as a result of recombination of doubly ionized cadmium ions with electrons, whereas IR transitions belong to neutral cadmium and are obtained as a result of recombination of singly ionized cadmium ions with electrons. Higher value of discharge current is required to create higher ionization stages, therefore, the optimum value of current is large for visible transitions compared to that for IR transitions. Since, recombination rate

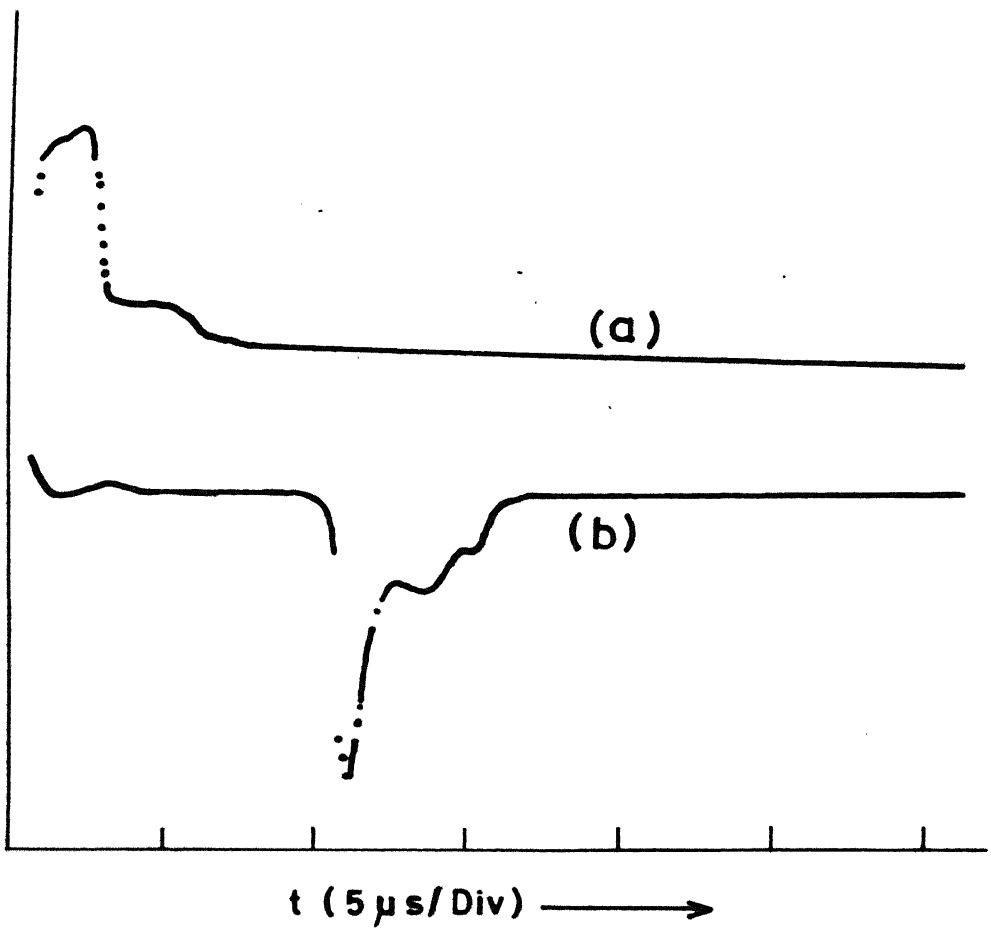

Fig. 29 Oscilloscope trace of
(a) Current pulse
(b) Laser pulse

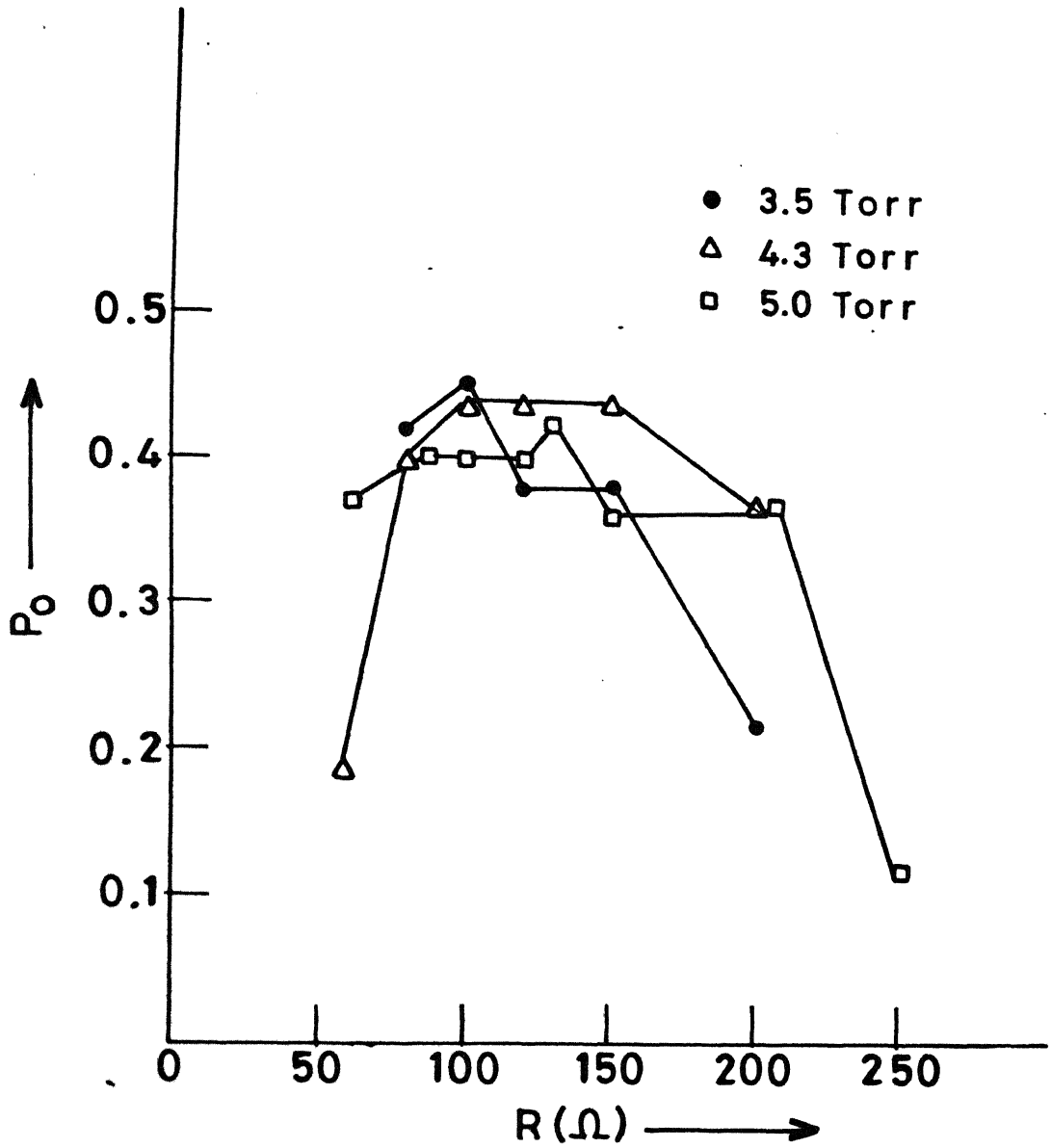

Fig. 30 Dependence of peak laser output power P_o on resistance R.

(eq 3) increases with increase in z, the charge on the ion. Therefore,laser pulse for the transitions corresponding to higher ionization stages will appear earlier than that from lower and neutral species [80].

c Effect of Pressure of Background Gas

Helium was used as background gas for visible transitions. Figs 31 and 32 show the variation of P_o with helium gas pressure. Laser output increases with the helium gas pressure, attains a maximum value and then decreases with further increase in pressure. Similar behaviour was observed for IR laser. For lower value of dumped energy ($\frac{1}{2}CV^2$), the optimum value of helium pressure was also low (Fig 31). With increasing length of the gain medium, for the same dumped energy, the optimum value of helium pressure decreases. This may be due to the fact that with increasing length of the gain medium, the input energy per segment decreases, therefore, initial electron temperature decreases and hence less cooling will be required to achieve population inversion. From above, one would expect that keeping the input energy same, laser action can be obtained at very low pressure and even in plasma expanding in vacuum for very large number of segments. As explained in Chapter 3, it is difficult to achieve laser action in vacuum, under recombination condition, because of faster rate of fall of electron density than that of electron temperature. With the increase in the number of segments, the energy per segment decreases, resulting in low

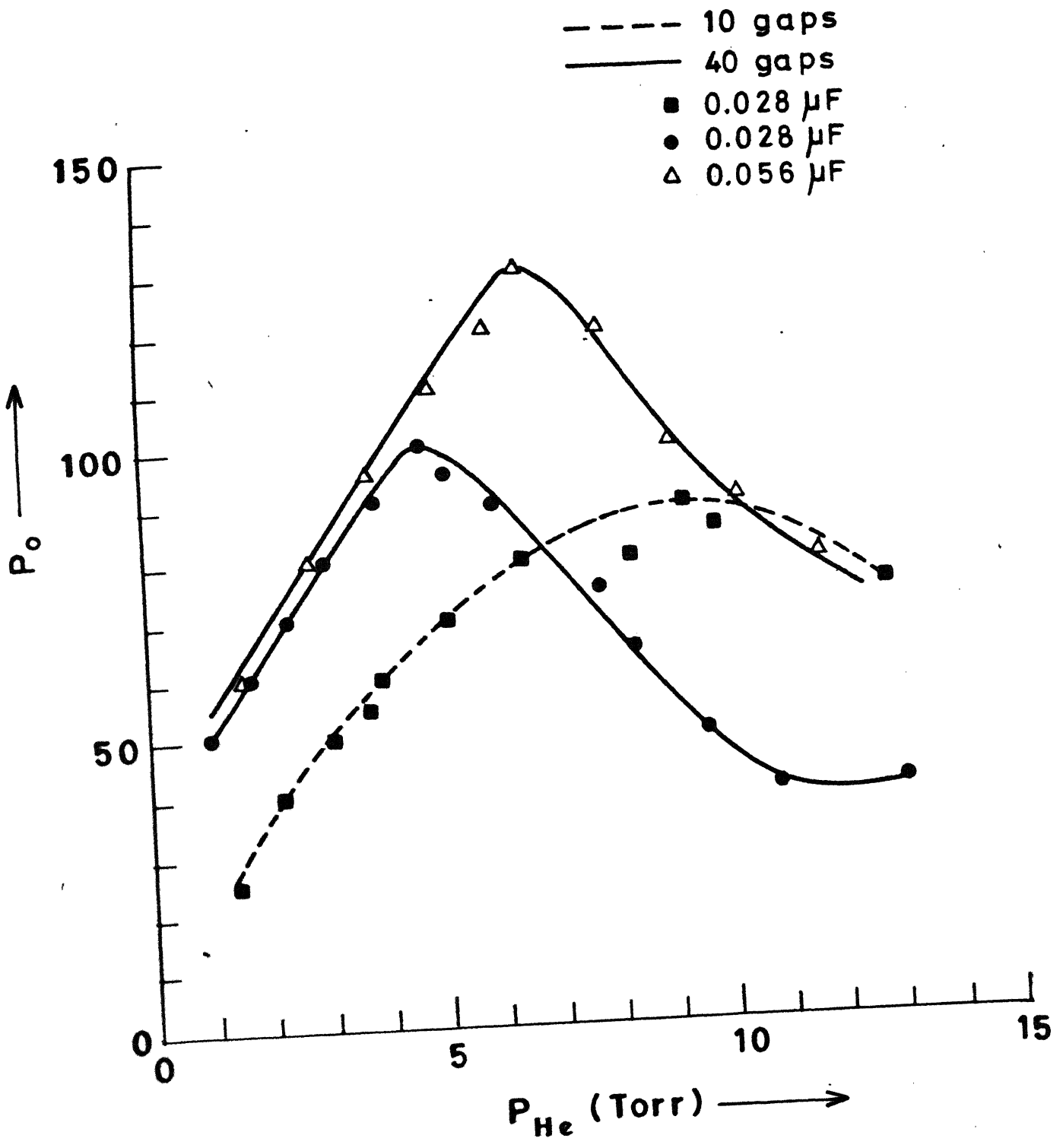

Fig.31 Variation of P_o with pressure of backgrou gas He for 10 and 40 segments.

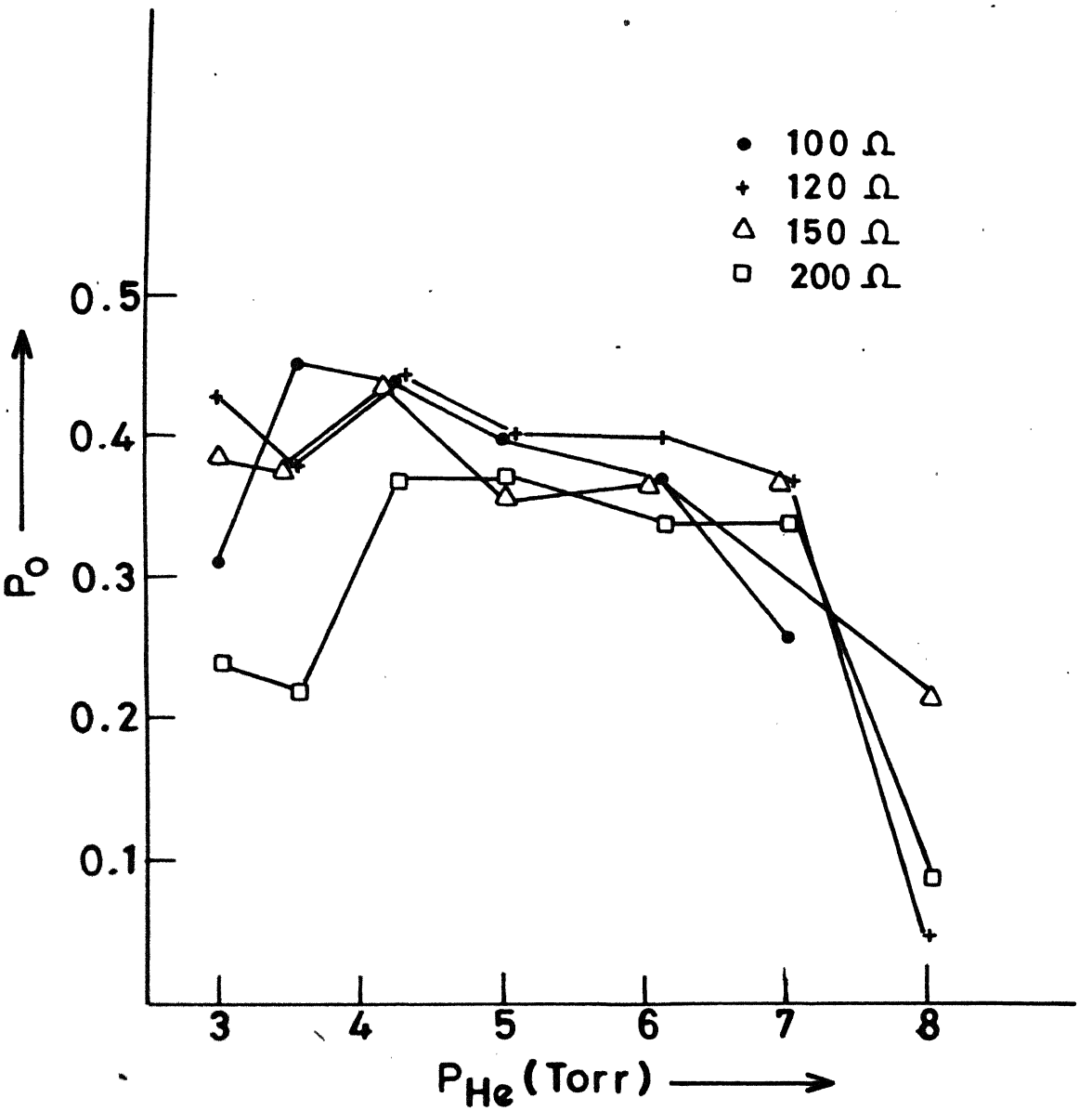

Fig. 32 Variation of P_0 with pressure of background gas He for 70 segments.

initial electron density. To get an optimum value of electron density with large number of segments it is required that the input energy per segment also increases.

An attempt was made to measure the small signal gain corresponding to 537.8 nm transition. Technique used was similar to that used for IR transitions. The experimental setup used is described in Chapter 2. The laser output with 10 and 40 plasma segments was very small and no conclusion could be drawn. However, extensive studies on gain for 70 segments were done. The maximum gain measured at 537.8 nm transition was 6.5×10^{-3} cm^{-1}.

In conclusion, we have observed laser action at 537.8 nm and 533.7 nm transitions of Cd II in SPER configuration in a sealed system. Characteristics of laser at 537.8 nm are presented. No appreciable effect on laser output is observed with two excitation circuits. By increasing the number of plasma segments, laser output increases. Delay is found to be less for visible transition than that for IR. The optimum value of current for best operation of laser is more than that for IR transitions. Small signal gain of the laser is estimated.

Chapter 5

GAIN CALCULATIONS

In this chapter, we have considered the use of simple electric network model for evaluatin population inversion and small signal gain of a recombination laser. Electron temperatures were estimated for Cd I and Cd II by estimating the gain and population inversion for a recombination laser. Gain and temperature based on our proposed model are compared with our experimental results [70,81].

The expression [30] for small signal gain (cm^{-1}) is given by

$$G_{u1} = \frac{c^2}{8\pi\nu^2} A(u,l)\, g(\nu)\, \Delta n_{u1}$$

For a Doppler broadened profile,

$$g(\nu) = \frac{2}{\Delta\nu_D}\left(\frac{\ln 2}{\pi}\right)^{1/2}$$

where

$$\Delta\nu_D = 2\nu \left(\frac{2kT}{Mc^2}\right)^{1/2} (\ln 2)^{1/2}$$

$$\therefore G_{u1} = 1.74 \times 10^{-6}\ \lambda^3_{u1}\ A(u,l)\sqrt{(M/T)}\ \Delta n_{u1} \qquad 18$$

where λ_{u1} is the wavelength of the transition considered (in cm), A(u,l) is the transition probability in sec^{-1}, approximated as

$$A(u,l) = 1.6 \times 10^{10}\ z^4/[u^3 l(u^2-l^2)]$$

M is the mass of the atom or ion under consideration (in amu), T is the ion temperature in °K (we can assume $T \approx T_e$) and

$\Delta n_{ul} = \frac{n_u}{g_u} - \frac{n_l}{g_l}$ is the population inversion density (cm^{-3})

where g's are the statistiical weights of the levels considered.

First, let us calculate the small signal gain under collisional recombination condition for hydrogen like transitions. In the quasi-steady state approximation, the density of a level u in a recombining plasma can be written [82] as

$$\frac{n_u}{n_E^{(u)}} = r_o(u) + r_1(u) \frac{n_1}{n_E^{(1)}} \qquad 19$$

where $n_E^{(u)}$ is the Saha equilibrium density given by

$$n_E^{(u)} = \frac{1}{2} g_u \left(\frac{h^2}{2\pi m_e kT_e}\right)^{3/2} n(z+)\, n_e \exp\left(\frac{E_H z^2}{u^2 kT_e}\right) \qquad 20$$

n_e and $n(z+)$ are the electron and ion density (cm^{-3}) respectively and $r_o(u)$ and $r_1(u)$ are functions of n_e and T_e, allowing for the departure from thermal equilibrium. The values of $r_o(u)$ and $r_1(u)$ are given in tabular form by McWhirter [82]. Defining the reduced population and temperature, respectively as $\eta = \frac{n_e}{z^7}$, $\theta = T_e/z^2$ (z scaling for hydrogen like ions). From plasma neutrality condition, we have

$$n(z+) = \frac{n_e}{z} = \eta z^6$$

Equation 20 can be rewritten as

$$n_E^{(u)} = \frac{1}{2} z^4 n(z+) \eta g_u \left(\frac{h^2}{2\pi m_e k\theta}\right)^{3/2} \exp\left(\frac{E_H}{u^2 k \theta}\right) \qquad 21$$

Generally the population density of the higher levels are closer

to those in LTE than those of lower levels are, i.e. with increasing i, $r_o(i)$ increases and approaches unity as a limit and $r_1(i)$ decreases and tends to zero, except for low lying levels in optically thick ions, therefore, eq 19 reduces to

$$n_u = r_o(u)\, n_E^{(u)} \qquad 22$$

From eqs 21 and 22 we get

$$n_u = \frac{1}{2}\, r_o(u)\, z^4\, n\, (z^4)\, f\left(\frac{h^2}{2\pi\, m\, k\, \theta}\right)^{3/2} \exp\left(\frac{E_H}{u^2\, k\, \theta}\right) \qquad 23$$

since $\Delta n_{ul} = \frac{n_u}{g_u} - \frac{n_l}{g_l}$

$$\Delta n_{ul} = 2.07 \times 10^{-16}\, z^{10}\, \frac{\mu^2}{\theta^{3/2}} \left[r_o(u) \exp\left(\frac{E_H}{u^2\, k\, \theta}\right) - r_o(l) \exp\left(\frac{E_H}{l^2\, k\, \theta}\right) \right] \qquad 24$$

Equation 24 can be used for evaluating population inversion and hence the gain. Based on eq 24 results for C VI are listed in Table 1. As expected the results agree with the experimental observations [10, 13].

A simpler way to calculate $r_o(u)$ is to consider the collisional processes in terms of passage of steady current through a network of linear conductors or resistors, originally proposed by Bates [66] and extended by Lawless [67]. In this model the collisional transitions from one level to another level are represented by resistor or conductor. The processes other than electron-atom collision are accounted by source terms which

represent the current introduced to the system. Each atomic level is represented by an electrical terminal to which the resistors and the source terms are connected as shown in Fig 33. The ionization and recombination rate constants can be determined only by total resistances between the continum level and the ground level. To develop an analogy with electrical circuit, let us consider the following collision processes

$A^+ + e + e \Leftrightarrow A_i + e$

$A^+ + e \Leftrightarrow A_i + h\nu$

25

$A_i + e \Leftrightarrow A_j + e$

$A_i + h\nu \Leftrightarrow A_j$

Let n_i be the population density of atoms in the ith level. The rate equation for each atomic level i and electron density are

$$\frac{dn_i}{dt} = n_e \sum_{j=1}^{M_m} (n_j k_{ji} - n_i k_{ij}) + n_e^3 K_{ei} - n_e n_i K_{ie}$$

$$+ \sum_{j=i+1}^{M_m} n_j A(j,i) + n_e^2 A_{ei} - n_i \sum_{j=1}^{i-1} A(i,j) \qquad 26$$

$$\frac{dn_e}{dt} = n_e \sum_{j=1}^{M_m} n_j (K_{je} - n_e^2 K_{ej}) - n_e^2 A_{ei}$$

where M_m is the highest excited atomic level, K_{ij} is the collisional rate constant for a transition from level i to j, A(i,j) is the Einstein Coefficient. A_{ei} is the rate constant for two body radiative recombination into level i, K_{ie}, K_{ei} are rate constants for collisional ionization from level i and three body recombination directly into level i.

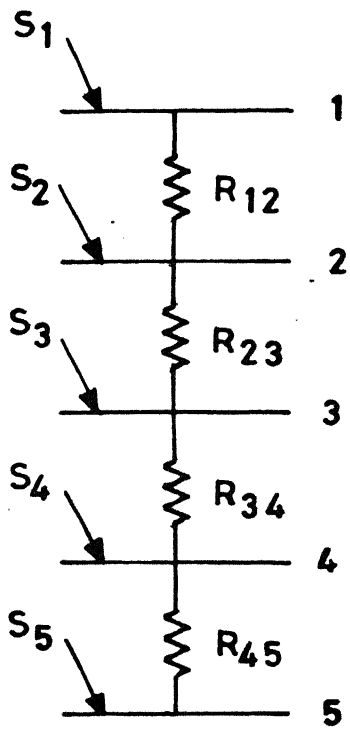

Fig. 33 Simplified circuit for collisional transitions between adjacent energy levels.

Rewriting eq 26 as

$$S_i + \sum_{j=1}^{M_m} (n_j K_{ji} - n_i K_{ij}) + n_e^2 K_{ei} - n_i K_{ie} = 0 \qquad 27$$

$$S_e + \sum_{j=1}^{M_m} (n_j K_{je} - n_e^2 K_{ej}) = 0 \qquad 28$$

Where S_i takes care of all the terms other than electron-atom collision. It is referred to as source term.

Defining the reduced populations for the atomic levels and free electrons as

$$v_i = \frac{n_i}{n_i^B} \qquad 29$$

$$v_e = \frac{n_e^2}{n_e^2 (N_{REF})} \qquad 30$$

where n_i^B is the Boltzmann population for the level i given as

$$n_i^B = \frac{g_i}{g_1} N_{REF} \exp\left(\frac{E_i - E_{H^2}}{kT_e}\right) \qquad 31$$

$n_e^2 (N_{REF})$ is the value that the Saha electron density would assume if the ground level density were N_{REF}, for hydrogen, one can write

$$n_e^2 (N_{REF}) = \frac{2}{g_1} N_{REF} \left(\frac{2\pi m_e kT_e}{h^2}\right)^{3/2} \exp\left(-\frac{E_H}{kT_e}\right)$$

Corresponding to the reduced populations, define the normalized rate constants as

$$W_{ij} = n_i^B K_{ij} \qquad 32a$$

$$W_{ie} = n_i^B K_{ie} \qquad 32b$$

$$W_{ei} = n_e^2 (N_{REF}) K_{ei} \qquad 32c$$

From the principle of detailed balance we have,

$$W_{i,j} = W_{j,i}$$

Using eqs 29, 30 and 32, eqs 27 and 28 can be combined to yield

$$\sum_{j=1}^{e} W_{i,j}\,(v_j - v_i) + S_i = 0 \qquad 1 \le i \le e \qquad 33$$

Each term in eq 33 can be interpreted as the current flowing from node j to node i through a resistor of conductance $W_{i,j}$ as shown in Fig 33. The current flowing through the resistor being given by $W_{i,j}(v_j - v_i)$. If S_i represents the current introduced to node i from external source, eq 33 can be interpreted as the conservation of current at node i.

Following Mansback and Keck [83], colllisional rate constants can be separated into a function of the lower atomic level multiplied by a function of higher atomic level, therefore, $W_{i,j}$ can be written as

$$\left.\begin{aligned} W_{i,j} &= L_i\, U_j \qquad i<j \\ W_{j,i} &= L_j\, U_i \qquad j \le i \end{aligned}\right\} \qquad 34$$

for hydrogenic levels L_i and U_i are given by

$$L_j = C(T)\,(2N_{REF}/g_i)\,\exp\left(\frac{-E_H}{kT_e}\right) j^{6.66}$$

$$U_i = i^{-3}\exp\left(\frac{E_i}{kT_e}\right) \qquad i \le j \le M$$

Define

$$\Omega_i = (U_i C_i + L_i D_i)^{-1}$$

$$A_i = \sum_{j=i}^{e} U_j v_j$$

$$B_i = \sum_{j=1}^{i-1} L_j v_j \quad i>0 \text{ and } B_1 = 0$$

$$C_i = \sum_{j=1}^{i-1} L_j \quad i>1, \quad C_1 = 0$$

$$D_i = \sum_{j=1}^{e} U_j$$

Using these parameters and eq 34, eq 33 becomes

$$\frac{v_i}{\Omega_i} = L_i A_i + U_i B_i + S_i \qquad 35a$$

for (i-1)th level

$$\frac{v_{i-1}}{\Omega_{i-1}} = L_{i-1}A_{i-1} + U_{i-1} B_{i-1} + S_{i-1}$$

using

$$A_i = A_{i-1} - U_{i-1}v_{i-1} \quad \text{and}$$

$$B_i = B_{i-1} + L_{i-1}v_{i-1}$$

it reduces to

$$\frac{v_{i-1}}{\Omega_{i-1}} = L_{i-1}A_i + U_{i-1}B_i + S_{i-1} \qquad 35b$$

defining a quantity J_i proportional to the net rate of transitions from all levels to level i and from i to all levels above and below i. Therefore,

$$J_i = \sum_{j=1}^{i-1} \sum_{k=i}^{e} W_{jk} (v_k - v_j) \qquad 36$$

using eq 34, eq 36 becomes

$$J_i = C_i A_i - B_i D_i \qquad 37$$

J_i depends on two unknowns A_i and B_i. However, from the conservation eq 33, it follows that J_i is sum over all the source terms,

$$J_i = \sum_{j=i}^{e} S_j \qquad 38$$

Eliminating A_i and B_i between eqs 35 and 37, we get

$$v_i - v_{i-1} = R_i J_i + \Omega_i S_i - \Omega_{i-1} S_{i-1} \qquad 39$$

where $R_i = \Omega_{i-1}\ \Omega_i\ (L_i U_{i-1} - L_{i-1}\ U_i)$

Equation 39 is a recursion relation, it gives the diffrence between the reduced population of adjacent levels i and i-1 in terms of R_i, Ω_i and Ω_{i-1} which are explicitly defined simple functions of the rate constants and the source terms in the form of S_i, S_{i-1} and J_i.

A solution of eq 39 is

$$v_i = v_e + \Omega_i\ S_i - \Omega_e\ S_e - \sum_{j=i+1}^{e} R_{i,j}\ S_j \qquad 40$$

where

$$R_{i,j} = \begin{cases} \sum_{k=i+1}^{j} R_k & j>1 \\ \\ R_{ji} & i<1 \end{cases} \qquad 41$$

For collisional recombination process the source terms in quasi-steady state are

$$S_i = \begin{cases} -\dfrac{1}{n_e}\dfrac{dn_e}{dt} & \text{for } i = e \\ 0 & \text{for } 1<i<e \\ -\dfrac{1}{n_e}\dfrac{dn_1}{dt} & \text{for } i = 1 \end{cases} \qquad 42$$

Also

$$\frac{dn_1}{dt} = -\frac{dn_e}{dt}$$

From eqs 40 and 42, it follows that reduced population for ground state and the excited state is given by

$$v_1 = v_e - R_{1e} S_e$$

$$= v_e - R_{1e}\left(-\frac{1}{n_e}\frac{dn_e}{dt}\right)$$

$$\text{or } \frac{dn_e}{dt} = n_e\left(\frac{v_1 - v_e}{R_{1e}}\right)$$

$$v_1 = v_e - R_{1e} S_e$$

$$= v_e + \frac{R_{1e}}{n_e}\frac{dn_e}{dt}$$

$$= v_e - R_{1e}\left(\frac{v_e - v_1}{R_{1e}}\right)$$

$$= v_e\left(\frac{R_{1e} - R_{1e}}{R_{1e}}\right) + \frac{R_{1e}}{R_{1e}} v_1$$

$$= v_e \frac{R_{11}}{R_{1e}} + \frac{R_{1e}}{R_{1e}} v_1$$

$$= r'_o(i)\, v_e + r'_1(i)\, v_1 \qquad 43$$

Equation 43 is similar to eq 19, following same reasoning as in eq 19, we have

$$v_1 = r'_o(i)\, v_e \qquad 44$$

where $r'_o(i) = R_{1i}/R_{1e}$,

From eqs 29, 30, 31 and 44 we have

$$n_u = 2.07 \times 10^{-16} \frac{g_u\, r'_o(u)}{T_e^{3/2}} n_e^2 \exp\left(\frac{E_H}{u^2\, kT_e}\right) \qquad 45$$

Thus an upper limit to the population of upper level u can be given by,

$$n_u = 3.13 \times 10^{-18} \frac{g_u\, r'_o(u)}{T_e^{1/2}\, \lambda^6_{ul}} \exp\left(\frac{E_H}{u^2\, kT_e}\right) \qquad 46$$

Now if one assumes that the lower level is empty, the problem reduces to evaluation of n_u in the expression for Δn_{ul}, and the gain expressin simplifies to

$$G_{ul} = 1.74 \times 10^{-6}\ \lambda^3_{ul}\, A_{ul}\, \sqrt{(M/T)}\, n_u \qquad 47$$

The computed values of n_u based on eqs 6 and 46, and G from eq 47 for hydrogen atoms at a temperature of 4000 °K are given in Table 2.

Let us consider the case of non-hydrogen like transitions. To consider the non-hydrogen like transitions z is to be replaced by z_{eff} given by $(I_P/I_{PH})^{1/2}$ where I_P is the ionization potential of the ion or atom under consideratin and I_{PH} is the ionization potential for a hydrogen atom ($I_{PH} = E_H$). The population of upper state can be written as

$$n_u = 2.07 \times 10^{-16} z^{10}_{eff} \frac{r_o(u)\ \pi^2\ g_u}{\theta^{3/2}} \exp\left(\frac{E_H}{u^2\ k\ \theta}\right)$$

$$= 2.07 \times 10^{-16} \frac{r_o(u)\ n_e^2\ g_u}{z_{eff}\ T_e^{3/2}} \exp\left(\frac{z^2_{eff}\ E_H}{u^2\ kT_e}\right) \qquad 48$$

Based on the above assumptions, gain for Cd I and Cd II transition is calculated in Table 3. The computed value of gain is found to be close to the experimentally observed results and to that of reported [42] earlier. The corresponding temperature are close to that predicted by Bohn and Schall [84] and our experimental observation [70].

In conclusion, we have shown that the value of $r_o(u)$ can be evaluated using a simple model of electric net work. We have evaluated the population density and gain for hydrogen, hydrogen like and non-hydrogen like transitions, which are in agreement with the previously quoted results. Based on our calculations, we have estimated the temperatures for Cd I and Cd II transitions. Results are close to the experimentally observed values.

Table 1

Calculated values of gain coefficient for C VI transitions

Tran-sition	θ(°K)	$n = 10^{12}$		$n = 10^{13}$		$n = 10^{14}$	
		n	G	n	G	n	G
4-2	2000	5.5(11)	3.32(-4)	–	–	–	–
	4000	9.1(10)	3.87(-5)	1.43(13)	6.05(-3)	–	–
	8000	1.2(10)	3.60(-6)	2.3(12)	6.92(-4)	-ve	–
	16000	2.3(9)	4.91(-7)	4.5(11)	9.58(-5)	-ve	–
	32000	4.8(8)	7.2(-8)	9.8(10)	1.44(-5)	5.0(12)	7.51(-4)
	64000	6.0(7)	6.37(-9)	1.73(10)	1.84(-6)	1.21(12)	1.29(-4)
	128000	-ve	–	4.24(5)	9.2(-12)	2.8(10)	2.11(-6)
	256000	-ve	–	-ve	–	-ve	–
4-3	2000	4.7(11)	0.017	-ve	–	–	–
	4000	6.0(10)	1.57(-3)	-ve	–	-ve	–
	8000	9.07(9)	1.66(-4)	2.24(11)	4.12(-3)	-ve	–
	16000	1.57(9)	2.05(-5)	1.67(11)	2.18(-3)	-ve	–
	32000	3.57(8)	1.24(-7)	4.8(10)	4.43(-4)	-ve	–
	64000	6.67(7)	4.33(-7)	1.14(10)	7.41(-4)	-ve	–
	128000	3.69(6)	1.70(-8)	1.45(9)	6.69(-6)	-ve	–
	256000	–	–	-ve	–	–	–
3-2	2000	7.7(10)	5.5(-4)	–	–	–	–
	4000	2.5(10)	1.37(-4)	2.32(14)	1.27	-ve	–
	8000	3.27(9)	1.27(-5)	2.12(10)	4.34(-3)	3.66(14)	1.42
	16000	7.06(8)	1.94(-6)	2.87(11)	7.9(-4)	7.8(13)	0.21
	32000	1.22(8)	2.37(-7)	5.02(10)	9.76(-5)	7.36(12)	0.014
	64000	-ve	–	5.92(9)	8.14(-6)	1.29(12)	1.77(-3)
	128000	-ve	–	-ve	-ve	5.03(10)	4.88(-5)
	256000	-ve	–	-ve	–	-ve	–

Read 5.5(11) = 5.5×10^{11} and 3.32(-4) = 3.32×10^{-4}, etc.

Table 2

Comparision of present calculations of gain and that obtained from Ref 82 for hydrogenic transitions.

(Temperature T_e = 4000°K)

				Based on eqs 46 and 47		Based on Ref 82	
Transition	λ (A°)	n_e	$F'_{ul}(\tau)$	η_{ul}	B	η_{ul}	B
2-1	1215	4.34(15)	0.064	1.55(14)	5.2	7.2(13)	2.39
3-1	1025	7.22(15)	0.509	3.16(13)	0.07	1.99(13)	0.044
3-2	6562	2.75(13)	0.509	4.52(8)	2.1(-4)	1.53(8)	7.12(-5)
4-2	4861	6.77(13)	0.8215	1.17(9)	3.89(-5)	9.37(8)	3.1(-5)
4-3	18750	1.18(12)	0.8215	3.54(5)	7.7(-7)	9.92(4)	2.16(-7)

Table 3

Calculated values of gain coefficient and estimated temperature for Cd I and Cd II transitions.

	θ(°K)	T_e(°K)	$r = n_u/n_e$	n_u(cm^{-3})	G(cm^{-1})
Cd I	3000	1968.3	1.47(-4)	2.93(8)	0.011
Cd II	8000	9856.8	6.1(-6)	4.79(8)	2.28(-3)

Chapter 6

CONCLUSION

We have used segmented plasma excitation and recombination configuration to observe laser action on $6p\ ^3P_2 - 6s\ ^3S_1$ at 1.40 μm, on $6p\ ^3P_1 - 6s\ ^3S_1$ at 1.43 μm, on $4f\ ^3F_4 - 5d\ ^3D_3$ at 1.65 μm transitions of Cd I and on $4f\ ^2F_{5/2} - 5d\ ^2D_{3/2}$ at 533.7 nm, on $4f\ ^2F_{7/2} - 5d\ ^2D_{3/2}$ at 537.8 nm transitions of Cd II based on eletron-ion recombination in a sealed discharge tube. Performance characteristics of visible and IR laser are presented with respect to resonator axis, current pulse, background gas pressure and the length of the gain medium. System described for the present work consisted of a special configuration of electrodes.

Two types of excitation circuits were used, i RC circuit and ii LC circuit. LC circuit with a fast rising edge was found to be more efficient than that of RC circuit.

Laser resonator was formed with two meter radius of curvature dielectric coated mirrors of high reflectivities. The optimum value of resonator axis was found to be 8 mm parallel to and away from the row of metal strips.

Laser action is observed in the afterglow region. Delay between the peak of laser pulse and current pulse is observed to be as much as 170 μs for Cd I and 30 μs for Cd II transitions. Delay increases with the increase in current. The optimum value

of current required for visible transitions is found to be higher than that for IR transitions.

Helium gas was used as background gas for most of the investigations. However, to see the effect of other background gases, we tried Ne, Ar and mixture of He-Ne. Helium being lightest of all the gases and of high ionization potential is found to be the best candidate. The electron cooling is inversely proportional to the mass of the background gas atom, therefore, with other gases, the electron cooling is not efficient. The effect was very clear with the mixtures of He and Ne gases where the laser output increases with the increase in proportion of helium gas in the mixture. Optimum value of helium pressure required is dependent on the transitions under consideration, number of plasma segments and the energy dumped in the system. With the increase in input energy, optimum value of helium pressure is found to increase. Laser output increases on increasing the number of plasma segments from 10 to 70 with identical input energy. However, there is a practical limit on the output power in this particular configuration. It is difficult to create simultaneously a large number of homogeneous plasmas. It may be due to nonuniform distribution of input energy in the segments. It may also be due to some delay in plasma formation in various segments. With the increase in number of plasma segments, keeping input energy same, optimum value of helium pressure decreases. Optimum helium pressure for various transitions observed is listed in Table 4.

Table 4

Optimum helium pressure for various observed laser transitions.

Transitions	Plasma segments	P_{He}(Torr)
4f $^2F_{7/2}$ – 5d $^2D_{5/2}$	10	9
(537.8 nm)	40	4.7
	70	4
4f $^5P_1$ – 6s $^5S_1$	40	12–14
(1.43 μm)	70	10–13
4f $^5F_4$ – 5d $^5D_3$	40	8
(1.65 μm)	70	8

Radial profile of IR laser was scanned and compared with theoretical fit. A double peak structure is observed in the radial profile. This is attributed to inhomogeneous expansion of plasma or simultaneous excitation of higher order modes or both effects present simultaneously.

Small signal gain of the laser was measured by introducing variable losses into the cavity. The gain estimated is 8.7 (-3) cm^{-1}, 7.1 (-3) cm^{-1} and 6.0 (-3) cm^{-1} for 1.65 μm, 1.43 μm and 537.8 nm transitions respectively.

Model based on simple electric network for computing small signal gain under collsional recombination is proposed. Using this model, gain for hydrogenic transitions was computed, the results were compared with existing detailed calculations. Our results are found to be in reasonable agreement with earlier reports. We have employed the proposed model for computing gain for observed Cd I and Cd II transitions. Results are listed in Table 5. The computed and estimated values are in agreement confirming the validity of theory. Plasma temperature is estimated by assuming thermal equilibrium and comparing the intensities of emitted visible cadmium transitions. The temperature is estimated to be in the range $0.5eV \leq T_e \leq 1eV$ for Cd I and $1eV \leq T_e \leq 2eV$ for Cd II. Temperature is also computed based on above model for Cd I and Cd II transitions and falls with in the experimentally observed values.

Table 5

Comparision of estimated and calculated values of small signal gain.

	T_e(eV)	G(cm^{-1})*	G(cm^{-1})**
Cd I	0.2	0.01	7.1(-3)
Cd II	1.0	2.3(-3)	6.0(-3)

* Theoretical
** Experimental

In order to gain more understanding on the working of a recombination laser, it is necessary to measure the plasma parameters; electron density and temperature, for various input parameters eg current pulse, pressure of the background gas. An extensive study of spatially resolved density and temperature should be made to find optimum value of plasma parameters for best operation of the laser.

In order to make commercially viable system based on configuration used, a further systematic study is to be undertaken. One of the major parameters which controls the laser output power is the coupling of the energy input to the metal plasma. It is requiried to optimize the configuration with respect to electrode structure, spacing between various segments, dimensions of the strips used. Length of the gain medium (i.e. large number of plasma segments) is to be increased/optimized to get large output. Though increasing the number of segments, the way we have done, increases the output, it introduces the problem of inhomogeneous distribution of energy. This also has effect on the radial profile (mode structure) of the laser output. We feel a better design for electrode configuration is to be looked into.

References

1. L I Gudzenko and L A Shelepin, Sov Phys JETP **18**, 998 (1964).
2. E L Latush and M F Sem, Sov Phys JETP **37**, 1017 (1973).
3. L I Gudzenko and L A Shelepin, Sov Phys Dok **10**, 147 (1965).
4. L I Gudzenko, A T Mamachun, and L A Shelepin, Sov Phys Tech Phys **12**, 598 (1969).
5. W L Bohn, Appl Phys Lett **24**, 15 (1974).
6. K Sato, M Shiko, M Hosokawa, H Sugawara, T Oda and T Sasakii, Phy Rev Lett **39**, 1074 (1977).
7. T Hara, T Ohgo, M Hamagapi and T Dote, Phys Lett **111A**, 285 (1985).
8. M Otsuka, Appl Opt **19**, 3904 (1980).
9. B F Gordiets, L I Gudzenko and L A Shelepin, Sov Phys JETP **28**, 489 (1969).
10. F E Iron and N J Peacock, J Phys B, Atom Molec Phys **7**, 1109 (1974).
11. R J Dewhurst, D Jacoby, G J Pert and S A Ramsden, Phys Rev Lett **37**, 1265 (1976).
12. R H Dixon and R C Elton, Phys Rev Lett **38**, 1072 (1972).
13. M H Key, C L S Lewis and M J Lamb, Opt Commun **28**, 331 (1979).
14. G J Pert, J Phys B, Atom Molec Phys **9**, 3301 (1976).
15. W W Jones and A W Ali, J Appl Phys **48**, 3118 (1977).
16. V A Bhagavatula and B Yaakobi, Opt Commun **24**, 331 (1978).
17. D D McGregor and M Mitchner, Phys Fluids **17**, 2155 (1974).

32. H Petschek and S Byron, Ann Phys (New York) 1, 270 (1957).

33. D E Golden and H W Bandel, Phys Rev 138 A14 (1965).

34. B F Gordiets, L I Gudzenko and L A Shelepin, Sov Phys Tech Phys 11, 1208 (1967).

35. R W P McWhirter, Plasma Diagnostic Techniques eds R H Huddlestone and S L Leonard, (Academic Press 1965) Ch.5.

36. H R Griem, Plasma Spectroscopy, (McGraw-Hill, New York, 1964.)

37. W T Silfvast, Appl Phys Lett 13, 169 (1968).

38. A Piper and C E Webb, J Phys D App Phys 6, 400 (1973).

39. M Brandt and A Piper, IEEE Quant Elect QE17, 1107 (1981).

40. G J Collins, J Appl Phys 44, 4633 (1973).

41. C J Willet, Introduction to gas lasers: population inversi mechanism, (Pergamon Oxford 1974).

42. W T Silfvast and O R Wood II, Opt Lett 8, 69 (1983).

43. W R Bernett Jr, Appl Opt Supplement on Optical M[illegible] 33 (1962).

44. P T Rumsby and J W M Paul, Plasma Phys 16, 247 (197[illegible]

45. E Hinnov and J G Hirschberg, Phys Rev 125, 795 (19[illegible].

46. V V Zhukov, V S Kucherov, E L Latush, M F Sem and G N Tolmachev, Sov Tech Phys Lett 2, 215 (1976).

47. M S Butler and J A Piper, Appl Phys Lett 42, 1[illegible]08 (1983).

48. M S Butler and J A Piper, Appl Phys Lett 45, 7[illegible]7 (1984).

49. M S Butler and J A Piper, Opt Lett 12, 166 (1[illegible]87)

50. C W McLucas and A I McIntosh, J Phys D Appl Phys **19**, 1189 (1986).

51. C W McLucas and A I McIntosh, J Phys D Appl Phys **20** 591 (1987).

52. R J DeYoung, W E Wells, G H Miley and J T Verdeyen, Appl Phys Lett **28**, 519 (1976).

53. L I Gudzenko, S S Filippov and L A Shelepin, Sov Phys JETP **24**, 745 (1967).

54. E M Campbell, R G Jahn, W F VonJaskowsky and K E Clark, Appl Phys Lett **30**, 575 (1977).

55. T Hara, K Kodera, M Hamagaki, M Matsunaga, M Inutake and T Dote, Jpn J of Appl Phys **19**, L606 (1980).

56. J J Rocca, Appl Phys Lett **47**, 1145 (1985).

57. T Hara, K Kodera, M Hamagaki, M Matsunaga, M Inutake and T Dote, Jpn J Appl Phys **19** L386 (1980).

58. K Sato, J Phys Soc Japan **43**, 1027 (1977).

59. W T Silfvast, L H Szeto and O R Wood II, J Appl Phys **50**, 7921 (1979).

60. C C Popovics, R Corbett, C J Hooker, M H Key, G P Kichn, C L S Lewis, G J Pert, C Regan, S J Rose, S Sadaat, R Smith, T Tonic and O' Willi (Preprint from RAL) (1987),

61. W T Silfvast, L H Szeto and O R Wood II, Appl Phys Lett **36**, 615 (1980).

62. W T Silfvast, O R Wood II and J J Macklin,, Appl Phys Lett **42**, 347 (1983).

63. A Khare and R K Thareja, J Appl Phys **XX** XX (1987).

64. R K Thareja and A Khare, Opt Lett **12**, 28 (1987).

65. J J Macklin, O R Wood II and W T Silfvast, IEEE J Quant Elect **QE18**, 1832 (1982).

66. D R Bates, Proc R Soc Lond **A337**, 15 (1974).

67. J L Lawless, J Appl Phys **55**, 3226 (1984).

68. F E Terman, Electronic and Radio Engineering (McGraw-Hill Kogakusha).

69. S A Schleusener and A A Reed, Rev Sc Inst **37**, 287 (1966).

70. A Khare, V Kumar and R K Thareja, Z Phys D (1987).

71. A N Zaidel, V K Prokof'ev, S M Raiskii, V A Slavnyi and E Ya Shreider, Tables of Spectral Lines (IFI/PLENUM, New York 1970).

72. C E Moore, Atomic Energy Levels Vol III (Nat. Stand. Ref. Data Ser, Nat. Bur. Stand. (US) 35/V.III Dec 1971).

73. A G Shenstone and J T Pittenger, J Opt Soc Am 39 219 (1949).

74. S Goldsmith, S Shalev and R R Boxman, Physica DE13 (1980).

75. D N Dulsovin, A S Tibilov and M K Shevtsov, Opt Spect 32 685 (1972).

76. E K Karabut, V S Mikhalevskii, V F Papakin and M F Sem, Sov Phys Tech Phys **14**, 1447 (1970).

77. Y Sugawara and Y Tokiwa, Jpn J of Appl Phys 9, 588 (1970).

78. W K Schuebel, Appl Phys Lett **16**, 470 (1970).

79. W T Silfvast and O R Wood II, J de Physique Colloque **C9**, 439 (1980).

80. A Khare and R K Thareja (Submitted).

81. A Khare and R K Thareja (Submitted).

82. R W P McWhirter and A G Hearn, Proc Phys Soc **82** 641 (1963).

83. P Mansbach and J Keck, Phys Rev **181**, 278 (1969).

84. W L Bonn and W Schall, 4th Int Symp Gas Flow and Chem. Lasers Stresa (Italy) 1982.

PHY-1987-D-KHA-CAD